UNIVERSITY OF OKLAHOMA

GRADUATE COLLEGE

STUDY ON THE EFFECTS OF TUBULAR RESTRICTIONS ON LIQUID LIFTING IN NATURAL GAS WELLS

A THESIS

SUBMITTED TO THE GRADUATE FACULTY

in partial fulfillment of the requirements for the

Degree of

MASTER OF SCIENCE

By

CAMILO ANDRES MATEUS RUBIANO

Norman, Oklahoma

2023

STUDY ON THE EFFECTS OF TUBULAR RESTRICTIONS ON LIQUID LIFTING IN NATURAL GAS WELLS

A THESIS APPROVED FOR THE

MEWBOURNE SCHOOL OF PETROLEUM AND GEOLOGICAL ENGINEERING

BY THE COMMITTEE CONSISTING OF

Dr. Hamidreza Karami Mirazizi, Chair

Dr. Xingru Wu

Dr. Pejman Kazempoor

© Copyright by CAMILO ANDRES MATEUS RUBIANO 2023

All Rights Reserved.

ACKNOWLEDGMENTS

I would like to express my deepest gratitude to my advisor, Dr. Hamidreza Karami, for his guidance, kindness, and unwavering support over the past three years. His encouragement to embrace every opportunity for learning and personal growth led me to pursue a dual master's degree. He not only motivated me to excel in my studies but also actively supported my involvement in extracurricular activities. My journey at the University of Oklahoma (OU) has been a life-changing experience, and it is thanks to the opportunity he gave me.

My appreciation and thanks to Dr. Pejman Kazempoor for being part of my committees for both petroleum and mechanical engineering. I am also grateful to Dr. Xingru Wu for his valuable feedback. Their suggestions and ideas served to enhance the quality of this work.

Special thanks to Jeff McCaskill, his assistance with the laboratory equipment at Well Construction Technology Center (WCTC) was fundamental for completing this project. Also, a big thank you goes to my friend Maziad Alsanea for sharing his knowledge and laboratory testing experience. I certainly enjoyed working with them and learned a lot from the hands-on work.

To my awesome wife, Camila Castillo, my life at Norman would not have been the same without you. Your love and support throughout this journey have been invaluable. I have learned and grown so much by your side, and I cannot wait to begin the next chapter of our life together.

To my parents, who have always gone the extra mile to provide me with the best, and to my brothers, for always pushing me to face new challenges and experiences, I extend my heartfelt gratitude. Also, I want to extend my thanks to my extended family who has helped me in one way or another while living abroad.

To my friends here at OU for their advice and support, especially to Laura Ortiz, Jhouly Osorio, Karan Shah, Cesar Vivas, Vanessa Rios, Carlos Lopez, Ducha Hapsari, Karelia La Marca, Sergio Garcia, Julio Rojas and Esteban Ugarte.

To my host family, Gloria and Mitch Burrus, you have been like angels since my arrival at OU as an exchange student. I really appreciate all that you have done for me and many other international students. Also, to the Colombian Student Association (COLSA) and, in particular, to Yoana Walschap, thanks for the warm welcome from day one and for the aid through scholarships.

To the University of Oklahoma and the Mewbourne School of Geological and Petroleum Engineering for all the resources provided. In particular, thanks to Katie Shapiro who has always been open to help.

To God for the amazing life opportunities that I have enjoyed.

TABLE OF CONTENTS

LIST OF TABLES

LIST OF FIGURES

ABSTRACT

Camilo Andres Mateus Rubiano

Study on the Effects of Tubular Restrictions on Liquid Lifting in Natural Gas Wells

Directed by Dr. Hamidreza Karami Mirazizi

Liquid loading is a common issue in natural gas wells, resulting in the accumulation of liquids in the well due to the inability of the gas to carry them to the surface. Various methods have been proposed to identify and address liquid loading, with no optimum solution. Several factors must be taken into account including location, costs and fluid properties. The use of partial tubing restrictions, namely inserts, was proposed about 2 decades ago, yet very limited investigation has been done about it.

Most of previous studies have been conducted using only air and water as fluids and have identified that inserts best performance is encountered at low v_{SL}. The present study involves the use of air and oil to evaluate the effectiveness of inserts at a range of conditions from annular to churn-slug flow. The measured parameters are pressure drop, liquid holdup, and video recordings of each test. The test matrix involves over 15 superficial gas velocities and 3 superficial liquid velocities. The effect of insert size and insert spacing is experimentally studied and models reported in the literature are benchmarked.

The results suggest that inserts are most effective at low v_{SL}, and in churn flow conditions. Their effects are diminished at low v_{Sg} ranges of slug flow and high v_{Sg} ranges of annular flow. It was found that the insert size is a relevant parameter in tests involving at least two inserts. The

1.5” insert displays a pronounced positive effect within a narrow v_{Sg} range, beyond which negative effects are observed. Tests using 1.75” inserts show a favorable performance for a wider range.

The spacing setup with the best performance is obtained by using: 2 inserts, followed by the cases with 1 insert. In the 2-insert configuration, significant improvements are achieved regarding liquid holdup, compared to the cases with a single insert. Also, for this configuration the frictional losses are not substantially increased, in contrast with the tests having three inserts. This method could offer an economical, passive, and effective solution for liquid unloading in gas wells.

CHAPTER 1. INTRODUCTION

Natural gas plays a crucial role in the global energy landscape. It accounts for about 40% of electricity generation in the United States, and around a quarter of electricity generation worldwide (Energy Institute, 2023; US Energy Information Administration, 2023). Natural gas has less carbon emission compared to most other fossil fuels, positioning it as a key component in the ongoing energy transition. Furthermore, it is used in the industrial sector to manufacture a variety of materials ranging from fertilizers to medical products. However, natural gas production comes with some key challenges that need to be addressed.

Liquid loading is a prevalent challenge in natural gas wells, especially as the pressure declines over time. At the initial stages of a gas well's life, the reservoir provides enough energy for the gas to reach the surface and carry the liquid water and condensate droplets with it. As the pressure naturally declines due to gas production, the multiphase flow pattern in the wellbore changes. This leads to the accumulation of liquids at the wellbore, hindered gas production, and a reduced well lifespan. There is yet no agreement in the initiation criteria for liquid loading prediction. However, most models align with either the droplet fallback or the liquid film reversal as the liquid loading mechanisms.

The applied methods in the industry to treat liquid loading in gas wells are called well deliquification techniques. Multiple such techniques have been implemented to resolve or handle liquid loading, including the management of production, injection of additional fluids, and the installation of expensive artificial lift systems. However, there is no proven optimal technology

for well deliquification due to various wellbore flow factors. Operators are constantly looking for newer, cheaper, and more efficient ways to keep the liquids from loading in the gas wells.

One of the methods recently that has been discussed in the literature is the use of partial tubing restrictions to promote droplet atomization and prevent the liquids from falling back. However, a challenge lies in identifying the operational range, where the implementation of these restrictions yields a positive net effect in unloading the well. The presence of inserts inherently causes additional frictional losses, while reducing the liquid holdup. It is crucial to understand the impacts of these restrictions on liquid-gas flow in the wellbore and characterize their optimum operating range.

1.1. Objectives

The main objective of this investigation is to examine the effects of partial tubing restrictions, namely inserts, on liquid loading in natural gas wells. The specific objectives of this study are presented below.

- Study the influences of gas and liquid rate combinations on two-phase flow, under the low liquid loading conditions in the presence of inserts in vertical tubes.
- Assess the locality and significance of partial tubing restriction effects by analyzing the spacing and size of the restrictions for two-phase flow in vertical tubes.
- Benchmark the existing two-phase flow models for vertical tubes, and examine the effects induced by presence of inserts in a flow model.

1.2. Scope of work

The scope of this work is the experimental investigation of two-phase flow behavior in a vertical tube, where partial restrictions are introduced. The objective is to identify the optimum range, where the presence of inserts can help with well deliquification. Also, the effects induced by the presence of inserts in an existing model for annular and churn flow are examined.

The tests were carried out in a 25-ft (7.6-m) long, 2-in. (0.0508-m) ID vertical flow loop designed to simulate a natural gas well. Air and Iso-par L oil were used for the gas and liquid phases, respectively. Three superficial liquid velocities were tested, 0.00167, 0.0033, and 0.01 m/s. The superficial gas velocities were tested in the range 2 to 16 m/s, to encompass both churn and annular flows. Inserts of 3 sizes were used at one or two locations along the test section, to assess the impact of both size and spacing of the inserts on the flow.

The data acquired and examined for each of the tests include liquid holdup, pressure drop, and visual recordings of flow behavior. The results were compared to the data available in the literature, and used to benchmark the existing commercial models.

1.3. Outline

The structure of this thesis is designed to provide a clear understanding of the effects of partial restrictions on liquid-gas flow in vertical tubes. Firstly, CHAPTER 2 provides a compilation of relevant literature addressing two-phase flow in gas wells, liquid loading issue, and technologies that have been proposed to deal with it. CHAPTER 3 presents an overview of the experimental facility where the tests of this study were conducted, along with details on the data acquired and the test matrix. CHAPTER 4 discusses the results of the experiments by examining the effects of insert size and spacing. Previously reported tests without inserts are used to configure a baseline

scenario that allows to determine the changes they induce. CHAPTER 5 compares the obtained results with available models. CHAPTER 6 presents the conclusions and recommendations of the investigation.

CHAPTER 2. LITERATURE REVIEW

Multiphase flow consists of the flow of a mixture of multiple phases of matter. The presence of various phases in a system leads to changes in pressure drop, flow stability and heat transfer rate, which in turn impact the operational characteristics (Faghri & Zhang, 2020). In some cases, the coexistence of various phases in a single system is intentional, while in others, it is an unintended yet unavoidable occurrence. In the case of wet gas production systems, three-phase flow is frequently encountered, as the heavier components of the gas condensate along with traces of water, influencing flow characteristics (Karami et al., 2016).

Various parameters influence flow behavior during hydrocarbon production, including the fluid properties, pipe diameter, inclination, and the flow rate. Since it is not feasible to have a single flow loop to handle all these conditions, multiple flow loops have been built around the world. Falcone et al. (2008) presented a review of facilities capable of conducting two and three-phase flow tests and highlighted the challenges of replicating hydrocarbon wells in lab.

Hanafizadeh et al. (2017) carried out air-water-oil flow tests and discussed the added complexities of three-phase flow theoretical analysis and some simplifying assumptions. Takano et al. (2023) conducted two-phase (gas-liquid) and three-phase (liquid-gas-solid) flow experiments. They provided an overview of some homogeneous-flow and separated flow models for calculating frictional pressure drops in two-phase flow and examined a few models for gas–liquid–solid flows. Yaqub et al. (2020) reviewed and discussed various experimental investigations in liquid-liquid-gas three phase flow, and some prediction models that have been proposed.

Two-phase gas-liquid flow is the most encountered multiphase flow in a variety of industrial applications. As such, most experimental studies and correlations proposed target this area. Introducing a third phase complicates modeling efforts and poses experimental validation challenges due to the demand for extra equipment in the facilities. The following sections will introduce the fundamentals of two-phase flow, with a focus on vertical pipes. The prediction models for liquid loading initiation are reviewed. Some approaches used to address this issue are discussed, while special attention is given to those involving the use of partial tubing restrictions.

2.1. Two-Phase Flow

Two-phase flow can exhibit different liquid-gas distributions in the pipe or flow patterns. This refers to the geometrical configuration of gas and liquid phases that flow inside a pipe. Gas and liquid rates, pipe inclination, and diameter greatly influence the flow pattern. Additionally, physical properties of the fluids, including density, viscosity, and surface tension may exert a discernible impact on the flow pattern, although their influences are typically less pronounced.

Barnea et al. (1980) proposed a flow pattern map for vertical pipes that has been widely used. In horizontal and near horizontal configurations, the flow pattern can be broadly classified as dispersed bubble flow, annular flow, intermittent flow, and stratified flow. In the vertical and sharply inclined configurations, the possible flow patterns are annular flow, churn flow, slug flow and bubble flow. The focus of this study is on two-phase flow in vertical pipes and most of the discussion will be centered around churn and annular flows. Figure 2.1 displays the flow patterns encountered in vertical and sharply inclined pipes.

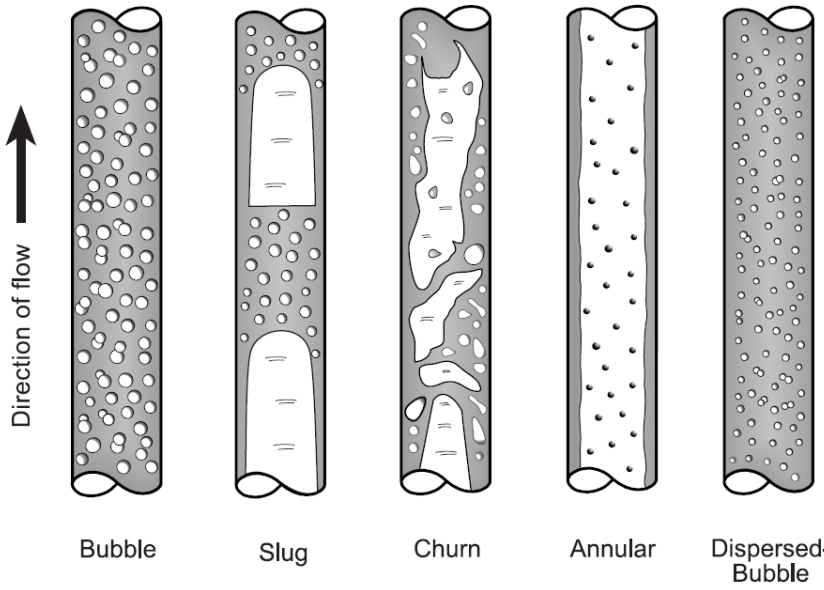

Figure 2.1 Flow patterns in vertical pipes. (Shoham, 2006)

Empirical correlations and mechanistic models are the principal modeling approaches used to study liquid-gas flow. The first one fits the experimental data to obtain an equation, which makes it simple, but limited to the ranges and conditions of the available data. The latter develops a physical model based on the conservation laws of mass, momentum, and energy, and makes use of closure relationships as needed. Mechanistic modeling is regarded as a more reliable and general approach combining physical laws and insights from experimental measurements.

The following paragraphs provide a concise overview of selected relevant multiphase flow models. Three empirical models are discussed, followed by three mechanistic models. Also, some closure relationships that can be used with the latter are presented.

Duns & Ros (1963) made use of dimensionless groups to construct a flow pattern map and define regions of validity for their correlations. The variables involved in these groups were superficial liquid velocity (v_{SL}), superficial gas velocity (v_{Sg}), liquid density (ρ_L), and surface tension (σ). Pipe diameter and liquid viscosity (μ_L) were also used to define other dimensionless

variables present in the calculations. Hagedorn & Brown (1965) correlation is widely used in the oil and gas industry. It was based on data from a 1500-ft deep vertical well, using various liquids to study the effects of viscosity, and considering three tubing sizes. They used the dimensional analysis of Duns and Ros to develop their correlation. Beggs & Brill's (1973) correlation is considered the first to account for all inclination angles. It is presented in an equation form, making it easily programmable. It was developed using experimental data collected at a testing facility, using water and air as the fluids, and two pipe diameters.

Aziz & Govier (1972) presented a flow pattern map for vertical flow and proposed a mechanistic model for two-phase flow in this configuration. The flow pattern is predicted using dimensionless variables and then considered for the calculation of pressure drop and liquid holdup. Ansari et al. (1994) made use of a previous study by Taitel et al. (1980) to predict flow patterns in upward two-phase flow. Then, models presented in previous studies (Caetano, 1985; Hewitt & Hall-Taylor, 1970; Sylvester, 1987) were used to calculate pressure gradient and liquid holdup, based on the flow pattern. The performance of this model was assessed using production data from over 1500 wells. Zhang et al. (2003) developed a unified model, commonly known as TUFFP model, based on the dynamics of slug flow. This model can predict pressure gradient, liquid holdup, flow pattern, and slug characteristics for all pipe inclinations.

Mechanistic models require the use of closure relationships where it is not feasible to obtain a physical model. Two variables of particular interest in this work are entrainment fraction (f_E) and interfacial shear stress (τ_I), due to their relevance in annular and churn flow patterns. The entrainment fraction corresponds to the ratio of the total liquid mass flowrate that is flowing as entrained liquid droplets in the gas core.

Oliemans et al. (1986) developed a correlation for entrained liquid fraction using the Harwell data bank. This databank encompasses over 10 studies and contains 728 data points for vertical flow. The pipe internal diameter ranges from 0.006 to 0.0318 m, while the pressure range is between 100 – 9000 kPa, and four different fluid systems are present. Table 2.1 shows the coefficients required to use the correlation.

$$\frac{f_E}{1-f_E} = 10^{\beta_0} \rho_L{}^{\beta_1} \rho_G{}^{\beta_2} \mu_L{}^{\beta_3} \mu_G{}^{\beta_4} \sigma^{\beta_5} d^{\beta_6} v_{SL}{}^{\beta_7} v_{Sg}{}^{\beta_8} g^{\beta_9} \quad (2.1)$$

Table 2.1 Coefficients in Oliemans' (1986) correlation

β_0	β_1	β_2	β_3	β_4	β_5	β_6	β_7	β_8	β_9
-2.52	1.08	0.18	0.27	0.28	-1.8	1.72	0.7	1.44	0.46

Azzopardi & Wren (2004) used water-air data with internal pipe diameters ranging from 0.024 to 0.05 m and pressures in the range of 100 – 300 kPa to predict f_E. The developed correlation can be expressed, involving three coefficients that depend on the superficial gas velocity. The two correlations obtained are as follows:

$$f_E = 0.47\, v_{Sg}{}^{0.16} v_{SL}{}^{0.35}, \quad if\ v_{Sg} < 5\ m/s \quad (2.2)$$

$$f_E = 0.6 v_{SL}{}^{0.35}, \quad if\ v_{Sg} > 5\ m/s \quad (2.3)$$

Interfacial shear stress (τ_I) models are key factors in the development of the momentum balance equation of annular and churn flow. However, due to the challenging nature of interfacial shear measurement, these correlations are not easy to develop and verify. Various efforts have been made to develop correlations for the interfacial friction factor (f_i), since this factor is the most difficult to obtain for the calculations. Equation (2.4) shows the relationship between f_i and τ_I.

$$\tau_I = \frac{1}{2} f_i \rho v^2 \quad (2.4)$$

Wallis (1969) provided a correlation for a simple analysis of annular flow depending on pipe diameter and liquid film thickness, as shown in Eq. (2.5). It is suggested that interfacial shear stress would increase with the film thickness (δ_L) due to the presence of larger waves.

$$f_i = 0.005\left(1 + 300 \frac{\delta_L}{d}\right) \quad (2.5)$$

Bharathan & Wallis (1983) developed a correlation using data from tests involving water-air churn flow. They made use of a dimensionless coefficient (d^*) to account for fluid properties as shown in Eqs. (2.6) and (2.7). A constant term is included to represent the friction factor corresponding to a smooth-walled pipe once the liquid film dissipates.

$$f_i = 0.005 + 10^{\left(-0.56 + \frac{9.07}{d^*}\right)} \left[\frac{d^*(1-\alpha)}{4}\right]^{\left(1.63 + \frac{4.74}{d^*}\right)} \quad (2.6)$$

$$d^* = d\sqrt{\frac{(\rho_L - \rho_G)g}{\sigma}} \quad (2.7)$$

The parameters involved in the calculation of d^* are liquid density (ρ_L), gas density (ρ_G), liquid surface tension (σ) and pipe diameter (d). The void fraction (α) is also used to obtain f_i.

Jayanti & Brauner (1994) examined experimental data from previous studies and suggested that Wallis (1969) correlation underestimates f_i, while Bharathan & Wallis (1983) correlation overestimates it. They proposed that the best estimation for the f_i would be the average of these correlations, as presented below in Eq. (2.8).

$$f_i = \frac{1}{2}\left(f_{i,B} + f_{i,W}\right) \quad (2.8)$$

Alsanea (2022) proposed a modification to the mechanistic model of Barnea (1986) for annular and churn flow, to account for the neglected liquid entrainment in the gas core. In the process of developing this model, various combinations of closure relationships for liquid entrainment and interfacial shear stress were evaluated. Given the inadequacy of the evaluated interfacial shear stress correlations and their impacts on the proposed model, a closure relationship was developed for f_i. This correlation was based on the collected experimental data and some data from previously reported studies. The correlation is a function of various parameters presented below in Eqs. (2.9) through (2.13). The coefficients involved in the f_i calculation procedure are shown in Table 2.2.

$$f_i = 10^{A+B*Re_{SL}} * \left(\frac{d^*(H_L)}{4}\right)^C \quad (2.9)$$

$$Re_{SL} = \frac{\rho_L v_{SL} d}{\mu_L} \quad (2.10)$$

$$A = X_1 + X_2 d^* \quad (2.11)$$

$$B = X_3 + X_4 d^* \quad (2.12)$$

$$C = X_5 + X_6 d^* \quad (2.13)$$

Table 2.2 Coefficients in Alsanea's (2022) correlation

Coefficient	Value
X_1	-0.33075
X_2	0.01896
X_3	1.029E-03
X_4	-6.052E-05
X_5	1.2305
X_6	0.03748

Chaves et al. (2022) conducted a comparative study using production data from 20 offshore wells using gas lift to assess the performances of several freely available multiphase flow models. Each of the wells was partitioned into two segments, wellbore, mostly near vertical; and flowline, near horizontal lines followed by riser. For the first segment 9 models were tested, while for the

latter 10 models were considered. This work provided insights to select the best models given the production system's flow parameters. Overall, Ansari's model had the best performance for wellbore segments. This model proposes a modified version of the model, previously developed by Barnea et al. (1986), for flow in vertical tubulars. Also, it was suggested that models tend to be more stable at higher flow rates, with higher errors found at low flow rates.

2.2. Liquid loading

Liquid loading is a prevalent challenge in natural gas wells, resulting from the accumulation of liquids at the wellbore due to insufficient gas energy to carry them to the surface. If not properly addressed, this phenomenon leads to changes in the multiphase flow pattern, hindered gas production, and a reduced well lifespan. Engineers employ various indicators to detect liquid loading, such as: erratic flow behavior, rise in casing pressure, production of liquid slugs, results from acoustic analysis, or pressure surveys suggesting an increased liquid level (Lea and Rowlan, 2019). Theoretical methods for predicting liquid loading include nodal analysis, flow pattern maps, and correlations for critical velocity based on the physics of liquid loading.

Numerous studies have attempted to establish a criterion for liquid loading onset, with no fundamental consensus. Most common models opt for either a liquid droplet fallback or a liquid film reversal approach.

Turner et al. (1969) developed and compared the performances of two models, one for droplet removal and one for film movement. The droplet removal model yielded the best results and served as the basis for subsequent studies. It considered the balance of forces on a spherical droplet with a drag coefficient of 0.44. A critical gas velocity was determined above which droplets

would move upwards. Based on the available data, a 20% adjustment from the initial formulation was suggested, leading to Eq. (2.14).

$$v_{Sg,c}(m/s) = 3.72\left(\frac{\rho_L - \rho_g}{\rho_g^2} g\sigma\right)^{\frac{1}{4}} \quad (2.14)$$

Coleman et al. (1991) tested Turner's model based on a dataset from low pressure gas wells. He concluded that the minimum or critical gas flowrate can be determined adequately using the initial Turner's formulation without the 20% adjustment. Nosseir et al. (1997) developed two models adopting Turner's basic concepts and considering the flow conditions. Li et al. (2002) proposed a flat droplet shape which changed the drag coefficient in Turner's model from 0.44 to 1, reducing the critical gas rate. Belfroid et al. (2008) proposed a modification to Turner's formulation to account for the effect of pipe inclination.

Multiple other studies agree that the mechanism by which liquid loading begins is film reversal. Hewitt and Hall-Taylor (1970) identified the "flow reversal" point at the transition where the liquid phase on the pipe wall began to creep down by reducing the gas rate. Barnea (1986) developed a model in which two criteria determined the transition between annular and intermittent flows. These criteria were liquid bridging and liquid film instability. Zabaras et al. (1986) analyzed the wall shear stress to better understand annular flow. They indicated that the change in film movement direction and onset of liquid loading corresponded to the point where wall shear stress changed from positive to negative.

In addition to the mechanistic modeling works, some studies have proposed empirical methods to identify liquid loading. Skopich et al. (2015) defined a criterion for liquid loading onset based on the liquid holdup (H_L). It corresponds to the superficial gas velocity (v_{Sg}) point for which the second derivative of H_L with respect to v_{Sg} is equal to zero. Alsanea et al. (2022) proposed a

method to identify liquid film movement by incorporating the H_L and total pressure gradient $\left(\frac{dP}{dL}\right)_T$ data. The liquid holdup is used to calculate the gravitational pressure gradient $\left(\frac{dP}{dL}\right)_G$, which is then subtracted from $\left(\frac{dP}{dL}\right)_T$ to obtain the frictional pressure gradient $\left(\frac{dP}{dL}\right)_f$. The liquid film reversal is then identified as the v_{Sg} where the $\left(\frac{dP}{dL}\right)_F$ changes from a negative to a positive value.

There is no specific optimal technology for well deliquification in all gas wells. Multiple factors must be considered, including the production rates, fluid properties, well location, energy availability, among other operational constraints. Decision trees have been proposed in previous studies (Devshali et al., 2019; Park et al., 2009) to aid in the selection of the most appropriate solution for each case. Below is a summary of various approaches based on a review by Tugan (2020) that examined several deliquification techniques, their advantages, limitations, and case studies of their applications.

- Cyclic or intermittent lift aims to keep the gas rate above critical values by permitting well pressure buildup during shut-in periods. It can be implemented easily.
- Foaming decreases interfacial tension and reduces liquid density by the generation of bubbles. This reduces the energy required to lift the liquids to the surface.
- Gas lift enhances gas velocity through the injection of additional gas. It unloads the liquid and lowers the density of the liquid-gas mixture in the tubing.
- Plunger lift harnesses the well energy in form of built-up pressure to lift the liquids to the surface, making it an economical artificial lift method. Its difference with intermittent lift is that it uses a plunger to reduce the liquid-gas slippage.
- Sucker rod pumps lift accumulated well liquids, thus allowing the gas to flow. However, they may require additional devices to prevent gas locking problems.

- Velocity strings are used to boost flow velocity by reducing the flow area. They need a careful design to balance the decrease of holdup and increase of frictional losses.

2.3. Effects of partial tubular restrictions

Partial tubing restrictions have been considered as one of the potential ways to combat liquid loading in gas wells. These restrictions can be introduced either naturally as tubular joints or as installed ring-shaped inserts. Yamamoto and Christiansen (1999) first investigated the use of restrictions in tubulars to enhance droplet formation and address the liquid loading faced in depleted natural gas wells. The factors considered in the study included insert design, gas flow rate, flow loop inclination, and the type of exit connection. It was found that the inserts were able to enhance the liquid lifting rate, and that the insert shape had a significant effect on its performance.

Putra and Christiansen (2001) conducted a comprehensive study on the effects of inserts by testing several parameters, including gas rate, liquid rate, insert shape, insert size, and number of inserts. The results indicated that inserts enhanced liquid lifting by preventing liquid fall back and promoting droplet generation. Models were developed and discussed of gas wells incorporating inserts and without inserts (Putra, 2000). They also found out that inserts display improved performances at lower liquid flow rates, and that there is an optimal operational gas flow rate range that depends on the liquid flow rate.

Veeken and Belfroid (2011) studied different methods to address liquid loading by delaying film reversal. One of the evaluated methods was the use of orifices or inserts with 1 mm thickness and varying internal diameters. They noted that the liquid film fallback is prevented by the insert and that the orifice promotes droplet entrainment into the gas core.

Alsanea (2022) carried out an in-depth study on the effects of liquid properties and inserts on liquid loading in natural gas wells. Three liquid rates and over 20 gas rates were assesed. Two-phase flow tests were performed using air with either water or oil, without and with inserts. For the latter case, three inserts were installed along the test section with a spacing between consecutive inserts of 1.85 m. The performances of several commercial software and common models were evaluated. It was concluded that the inserts exhibit their best performances at lower liquid rates and in the moderate to low gas rate region of churn flow. Furthermore, it was explained that the pressure drop is impacted in the presence of inserts in two ways, a reduction of gravitational losses and an increase of the frictional losses. Within the optimum range of inserts, the improvements in gravitational losses dominate and result in a positive performance. Table 2.3 shows a summary of the studies addressing the inserts as a well deliquification technique.

Table 2.3 Studies addressing liquid loading issues by using inserts

Study	Fluid rates	Insert characteristics	Other parameters
Yamamoto & Christiansen (1999)	v_{Sg}: 8, 10, 12.5, 14.5 m/s $v_{SL:}$ 0.0016, 0.0032, 0.0048, 0.0064 m/s	Slitted disk, toothed disk, perforated toothed disk, and open disk ID 1.125”, 1.375”	Water-air Inclination: 0°, 5.3° Pipe ID: 1.5”
S. Putra (2000); S. Putra & Christiansen (2001)	v_{Sg}: 2 – 12.2 m/s v_{SL}: 0.0007, 0.0015, 0.0075, 0.0117 m/s	Slitted disk, open disk ID 0.9”, 1.125”, 1.375”	Water-air Inclination: 0° Pipe ID: 1.5” Insert spacing
Veeken & Belfroid (2011)	v_{Sg}: 2 – 40 m/s v_{SL}: 0 – 0.0884 m/s	Open disk ID 0.63”, 0.512”, 0.236”	Water-air Inclination: 0° Pipe ID: 0.787”
Alsanea (2022)	v_{Sg}: 1 – 28 m/s v_{SL}: 0.0033, 0.01, 0.02 m/s	Open disk ID 1.5”, 1.75”	Water-air and Oil-air Inclination: 0° Pipe ID: 2”

2.4. Summary of Literature Review

Multiphase flow study is required to understand and address the challenges at various industries. It is, however, not a simple task and theoretical approaches are not feasible in most cases, due to the interaction of several factors at the same time. Mechanistic models provide a better representation of the systems than empirical correlations. Some relevant empirical and mechanistic models on vertical liquid-gas flow were presented in this chapter, along with the closure relationships used to incorporate features for which a physical model cannot be developed.

In natural gas wells, liquid loading is an issue that arises as the pressure declines and liquid accumulates in the bottom of the well. There is no clear agreement on the initiation criteria of liquid loading. Experimental and theoretical studies on liquid loading are reviewed. Some of the methods implemented to address this issue are discussed with particular emphasis on those involving the use of partial tubing restrictions, namely inserts. Previous studies have suggested that inserts have the capacity to prevent liquid film fallback and promote droplet entrainment. However, a challenge lies in identifying the operational range, where the implementation of restrictions yields a net positive effect in unloading the well. This work aims to bridge this gap in the literature and improve the understanding of how inserts impact the gravitational and frictional pressure losses of upward flow in vertical tubes. The objective is to identify the optimum operational window and parameters in applying the inserts.

CHAPTER 3. EXPERIMENTAL PROGRAM

As previously discussed, it is required to combine physical models with experimental studies to better understand two-phase flow dynamics. This chapter focuses on the latter and discusses the experimental program of the study. First, a description of the facility and the instrumentation used to collect measurements is provided. Then, the testing procedure is outlined in detail, followed by a description of the data processing algorithm and the test matrix.

3.1. Experimental Facility

An experimental facility located at the Well Construction Technology Center of the University of Oklahoma was adapted to conduct the two-phase flow tests of this study. The tests were carried out in a 25-ft long, 2-in. ID vertical flow loop, designed to simulate a natural gas well. The test section consists of acrylic pipes connected by Straub clamps at three locations. Inserts of 0.12” thickness, acting as partial tubing restrictions, are installed in up to two of these locations. Figure 3.1 shows an insert with a quarter coin for reference on its dimensions.

Figure 3.1 An insert used as a partial restriction, with a coin for size reference

Figure 3.2 shows the schematic of the facility used for this study. The facility includes the liquid and gas inlet lines, test section, and a return line to the oil tank. The locations of the inserts are numerated from the bottom to the top of the test section and referred to in the next sections.

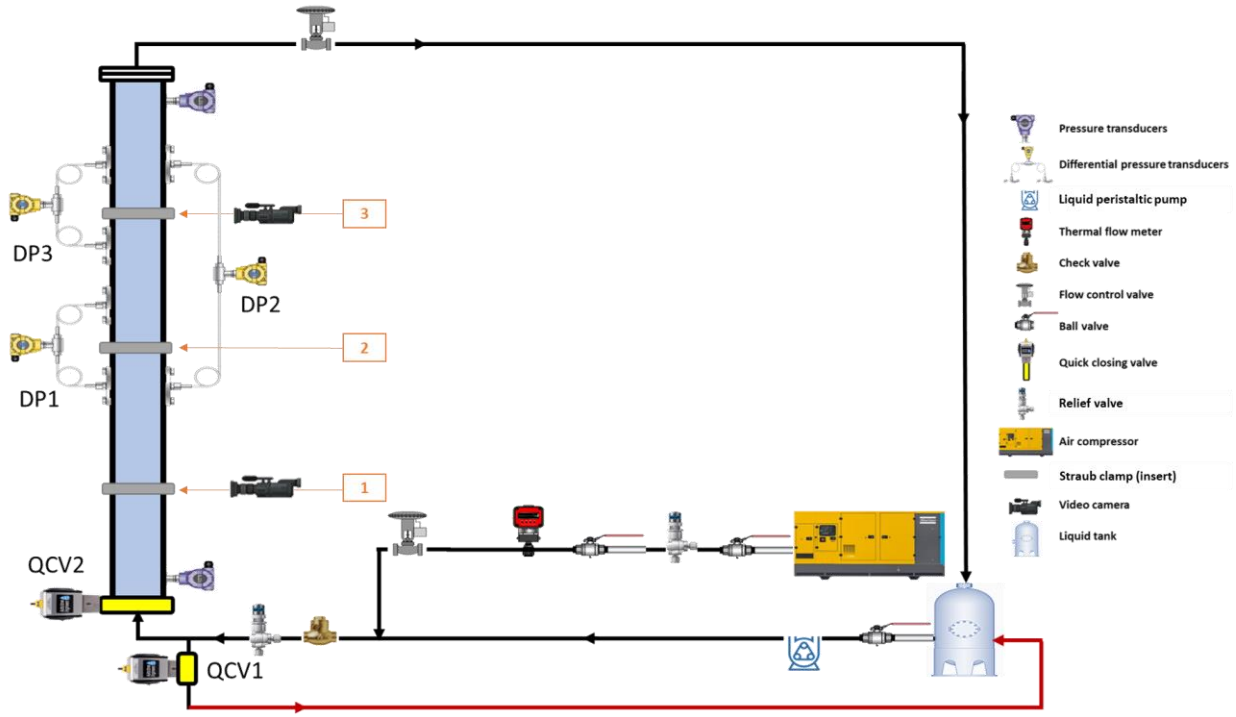

Figure 3.2 Schematic of facility. (Alsanea 2022)

The two-phase flow tests were carried out using oil for the liquid phase and air for the gas phase. Table 3.1 shows the properties of the tested fluids. To ensure proper mixing of the inlet fluids, a specially designed tee is connected at the base of the test section. After flowing through the test section, the fluids are routed back to the tank via a return line. This configuration enables the recirculation of the liquid while allowing the gas to vent into the atmosphere. The pressure is maintained below the facility's allowable pressure limit of 310 kPa (30 psig) using two relief valves, one at the inlet of the test section and the other after the air flow meter. Since the liquid tank is open, the outlet pressure is fixed at atmospheric pressure. A detailed explanation of the equipment and instrumentation involved in this experimental facility is covered by Alsanea (2022).

Table 3.1 Fluid properties at standard conditions

Fluid	Temperature (°C)	ρ (kg/m^3)	μ (cP)	σ (dynes/cm)
Air	15	1.225	0.0018	-
Iso-Par L Oil	15	760	1.27	24

Figure 3.3 shows an insert installed in the connection of two pipes in the experimental flow loop. The Straub clamp will then be mounted over this insert to keep it in place and maintain a proper connection through the test section. The distance between consecutive Straub clamps, which accommodate the inserts, is 1.85m (6.1 ft).

Figure 3.3 Insert installed between two pipes in the test section with Straub clamp unadjusted

The inserts were made using a 3-D printer, METHOD MakerBot, and carbon fiber-reinforced nylon. The design was accomplished using AutoCAD 2022, characterized by 0.12 in thickness, 2.5 in outside diameter (OD), and various internal diameters (ID). The tested IDs were chosen based on the range of common tool joints for 2 in tubings. OD was set to match the outer diameter of the acrylic pipe, while the thickness matched the one used in the previous study by Alsanea (2022).

3.2. Testing Instrumentation

A proper analysis of two-phase flow experiments requires obtaining data from various parameters. In this study, measurements of gas and liquid flow rates, pressure drop, and liquid holdup, along with video recordings were collected for each test.

A rotary screw compressor capable of delivering air at up to 2718 m^3/h and 800 kPa (100 psig) is used to feed gas to the facility. A thermal mass flow meter, calibrated for the range of 0–550 kg/hr (0–1200 lb/hr) and a control valve are used to regulate the air flow into the test section. The flowmeter generates a signal output ranging from 4 to 20 mA, which is then transformed into a voltage in the range of 0-10 volts using a resistor. These readings are sent to the data acquisition (DAQ) system and transmitted to the computer. The details of the calculations are presented in the following section.

The oil is stored in a tank with a capacity of 380 L. A peristaltic pump, shown in Figure 3.4, with a maximum flowrate of 2.9 L/min is connected to the tank and used to provide liquid for the experiments. The pump uses a flexible tube and rotating rollers to push fluids without direct contact with mechanical parts, ensuring purity and reliability. The flowrate was manually set before each test.

Figure 3.4 Peristaltic pump used to flow liquid into the test section

Pressure transducers (PT) with pressure ranges 0 – 310 kPa (30 psig), located at the inlet and outlet of the test section, serve to obtain an average pressure drop through the whole test section. The distance between them is 7.22 m (23.7 ft).

Pressure changes across specific sections are measured using differential pressure transducers, providing more accurate results within narrower pressure ranges. Differential pressure transducers (DP) measure pressure gradients by comparing the pressures of their two end taps. To ensure accurate readings, the tap lines must be filled using the same non-compressible fluids. The procedure presented in the next section explains how to keep these lines filled. DP1 has a range of 0–40 kPa and is situated 3.48 m from the base of the test section covering a length of 0.96 m (38 in). DP3 has a range of 0–10 kPa and is situated 5.3 m (17.5 ft) from the base of the test section. These two are supposed to obtain measurements of the pressure drop across the inserts mounted at the middle and upper Straub clamps. The longest section is covered by DP2, 2.82 m (9.25 ft). This DP has a range of 0–50 kPa and is situated starting at 3.48 m (11.4 ft) from the base of the test section. Figure 3.5 shows the existing DP sensors and the filled purge lines with liquid.

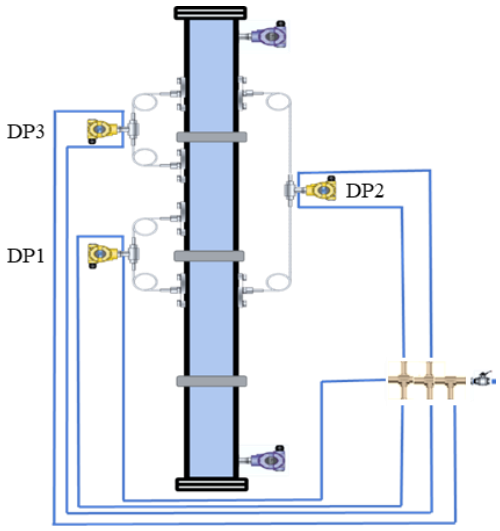

Figure 3.5 Schematic of the existing DP sensors and filled purge lines (Alsanea 2022)

Quick closing valves (QCV) are incorporated into the setup for safety and measurement purposes. The QCV at the base of the test section traps the liquids at the end of each test to obtain an average liquid holdup. The other QCV, which is closer to the fluid mixing tee, opens at the end of the test to return the incoming liquids and prevent pressure buildup. These QCV's open and close in a fraction of a second using pneumatic actuators, which receive an electrical signal from the data acquisition system at the beginning and end of each test.

Two cameras, GoPro Hero 9 Black, are used to record the flow behavior during the experiments. One of them is placed at the height of the lower Straub clamp, and the other is placed at the height of the upper Straub clamp, using a gooseneck clamp. These locations are selected based on the placement of inserts. Figure 3.6 depicts the top section of the test facility and some of the instruments used such as one of the cameras and two DPs.

Figure 3.6 Instruments near the top section of testing facility

An OMEGA multi-function I/O DAQ system is used to send and receive signals from the various instruments involved in the facility setup and a desktop computer. A LabVIEW program is used to interface with the OMEGA system and define the data acquisition tasks required. In particular, the air flow rate is regulated through a PID (Proportional Integral Derivative) algorithm, which sends a signal to adjust the opening of the gas control valve to match the set flow rate. Figure 3.7 shows a picture of the DAQ card and the power supply setup.

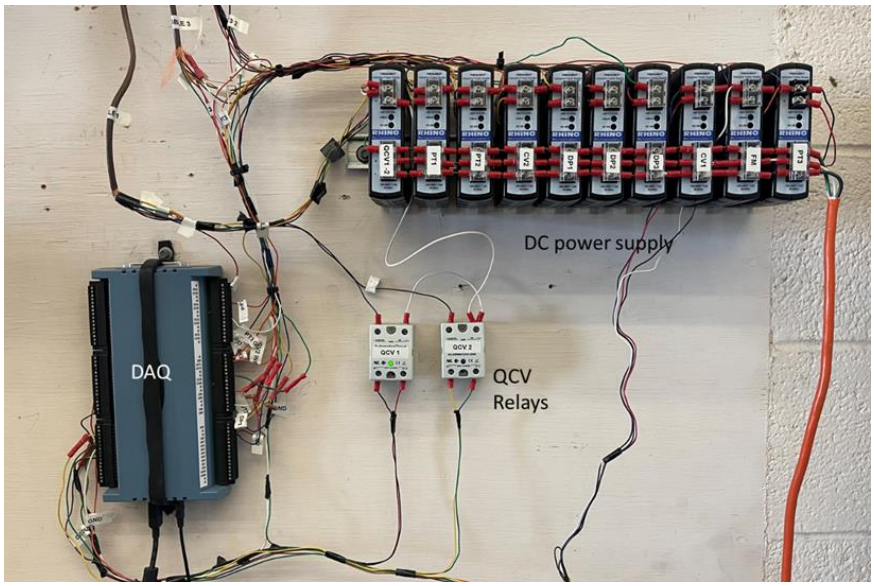

Figure 3.7 DC power supply, QCV relays and Omega DAQ

Control charts are generated within LabVIEW to provide real-time feedback and monitor the experiments. At the end of each test, the collected data are compiled in a comma-separated values file (.csv), which is later processed. A snapshot of the graphical source code or "block diagram" of the LabVIEW program, used to run the tests, is displayed below in Figure 3.8.

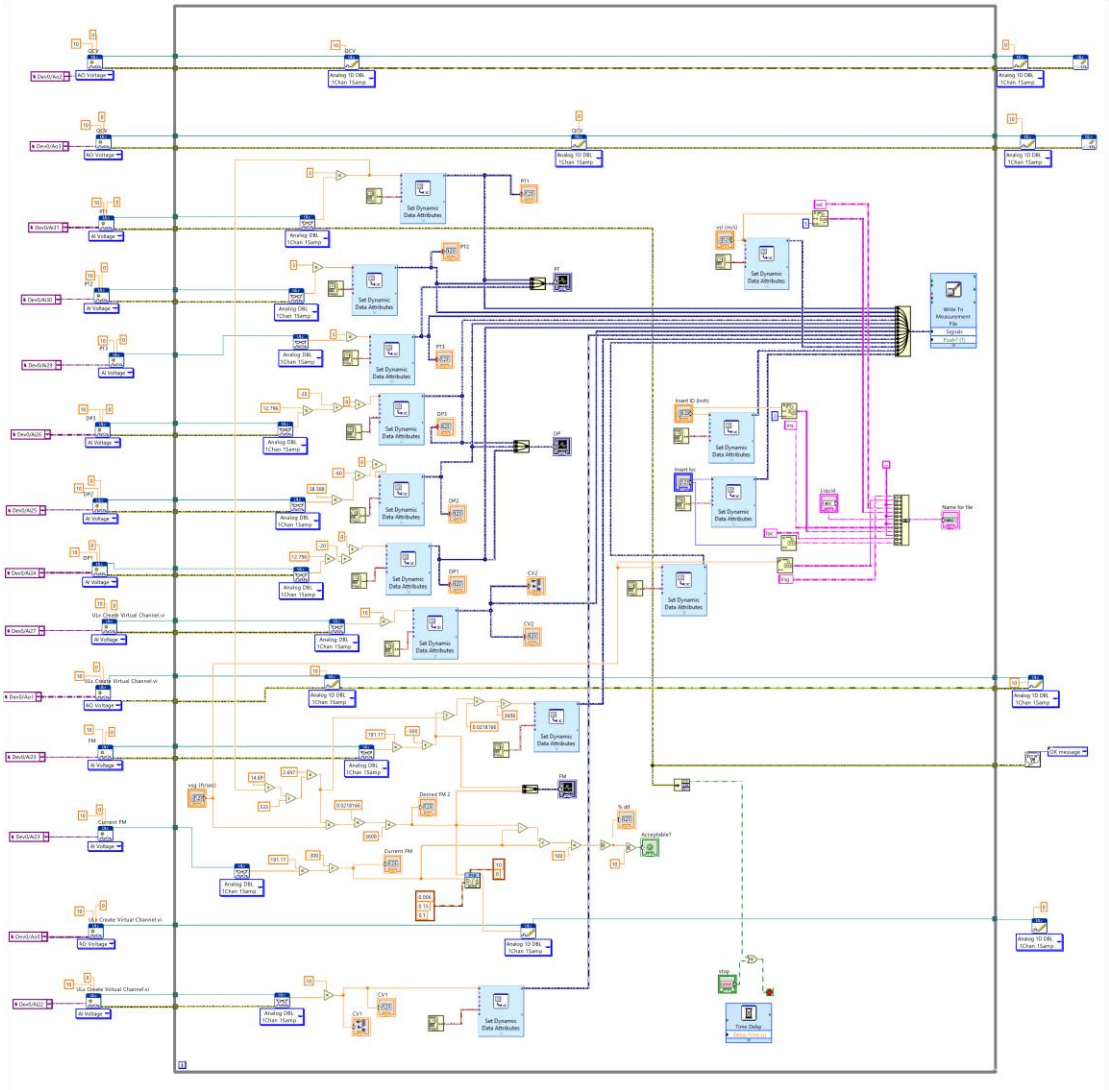

Figure 3.8 LabVIEW graphical source code for running experiments

3.3. Experimental Procedure

The following experimental procedure was followed in this study to carry out the experiments in a safe, repeatable, and accurate manner:

1. Open the purge line valves and the liquid supply valve, allowing the liquid to flow into the DP purge lines.
2. Check for air bubbles in the purge lines. Once they are filled with liquid, close the purge line valves, and stop the liquid supply.

3. Open the air supply valve for the QCV's, including the main air supply valve and the two air valves located before the tee between the liquid pump and the air lines.
4. Connect the hose to the air compressor. Turn on the compressor, make sure the oil level and fuel are enough for uninterrupted tests and load it up.
5. Connect the DC power supply cord to the AC power supply.
6. Turn on the GoPro camera and check for battery and storage before attaching it to the gooseneck for visual observations.
7. Start the LabVIEW program and input the desired superficial air velocity. Document other conditions of the test that are adjusted manually, such as pump liquid rate, insert size and location. Run the pump at the desired liquid flowrate.
8. Record videos of the test section when pressure and mass rates are attained and stabilized. This process takes between 20 – 40 minutes for each test.
9. Stop the LabVIEW program and the liquid pump. The QCV at the inlet of the test section automatically traps the liquid and the other QCV opens to prevent any pressure buildup.
10. Measure the liquid holdup and take a picture for evidence. Include the holdup level in the output .csv file created by LabView for the same test.
11. Repeat steps 7 – 10 for the desired gas and liquid flow rates.
12. When no more tests are planned, shut down the liquid pump and close all the valves.
13. Vent all the air in the air lines to avoid any pressure buildup that could cause damage. Unload the compressor and shut it off. Remove the air supply hose from the compressor.
14. Close LabVIEW, remove the power supply cord and dismount the GoPro cameras.

Figure 3.9 shows a snapshot of the front panel of the LabView program with a sample test beginning. This panel serves to run and monitor the experiments, and aids in determining when a steady state condition has been reached.

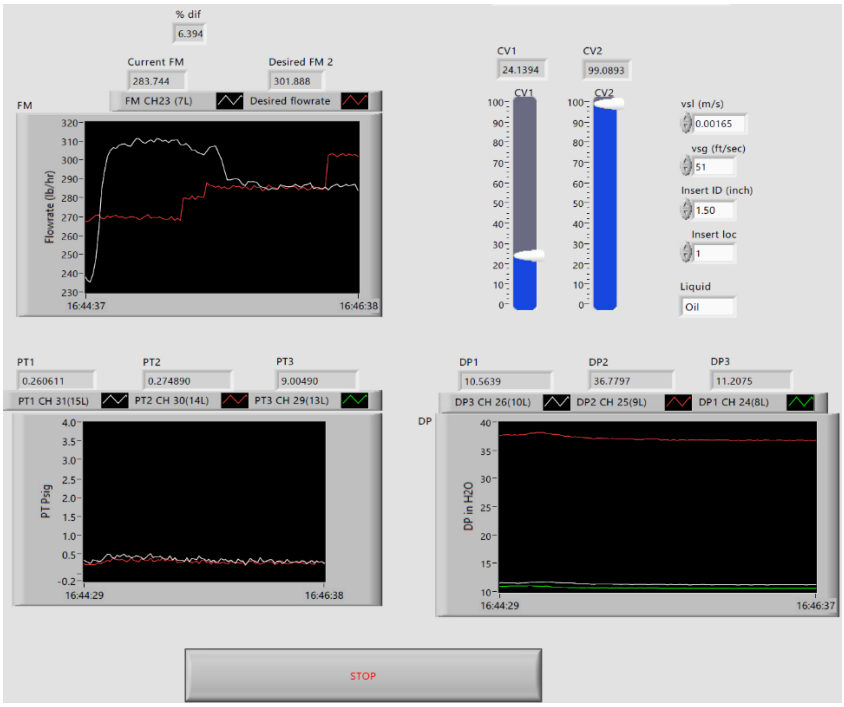

Figure 3.9 Snapshot of LabView during a sample test

3.4. Data Analysis

The utilized instrumentation allows recording up to 8 data points per second on each test. With over 250 tests conducted, and an average time of 30 minutes per test, the use of programming becomes necessary to effectively handle the data collected. Python 3.10.12 programming language is used to automate the preprocessing of the collected data. A step-by-step explanation of how this is achieved is presented here. Figure 3.10 shows a flowchart diagram to visualize this process.

1. Data acquisition: Retrieve .csv files corresponding to the experimental data. Raw files are generated at the end of each test, containing data from pressure transducers, while the liquid holdup measurements are added manually. Some tests are repeated.

2. Data validation: Files are validated to ensure they correspond to experimental tests.
3. Data integration: Validated .csv files are merged into a single comprehensive data frame
4. Revising columns: Additional columns are computed to facilitate the filtering of data.
5. Data inspection: Data quality is ensured by creation of plots for visual examination.
6. Steady-state data extraction: The data specific to the last few minutes of each test, representing steady-state conditions, are isolated and retained for further analysis.
7. Statistical analysis: Mean values, standard deviations, and coefficients of variation are calculated. Then, data uncertainty is determined considering instrument specifications.
8. Pre-processed data: A data frame is generated containing a single row per test. This includes mean values and uncertainties of the measurements. The data frame is then exported for advanced data exploration and visualization using PowerBI.

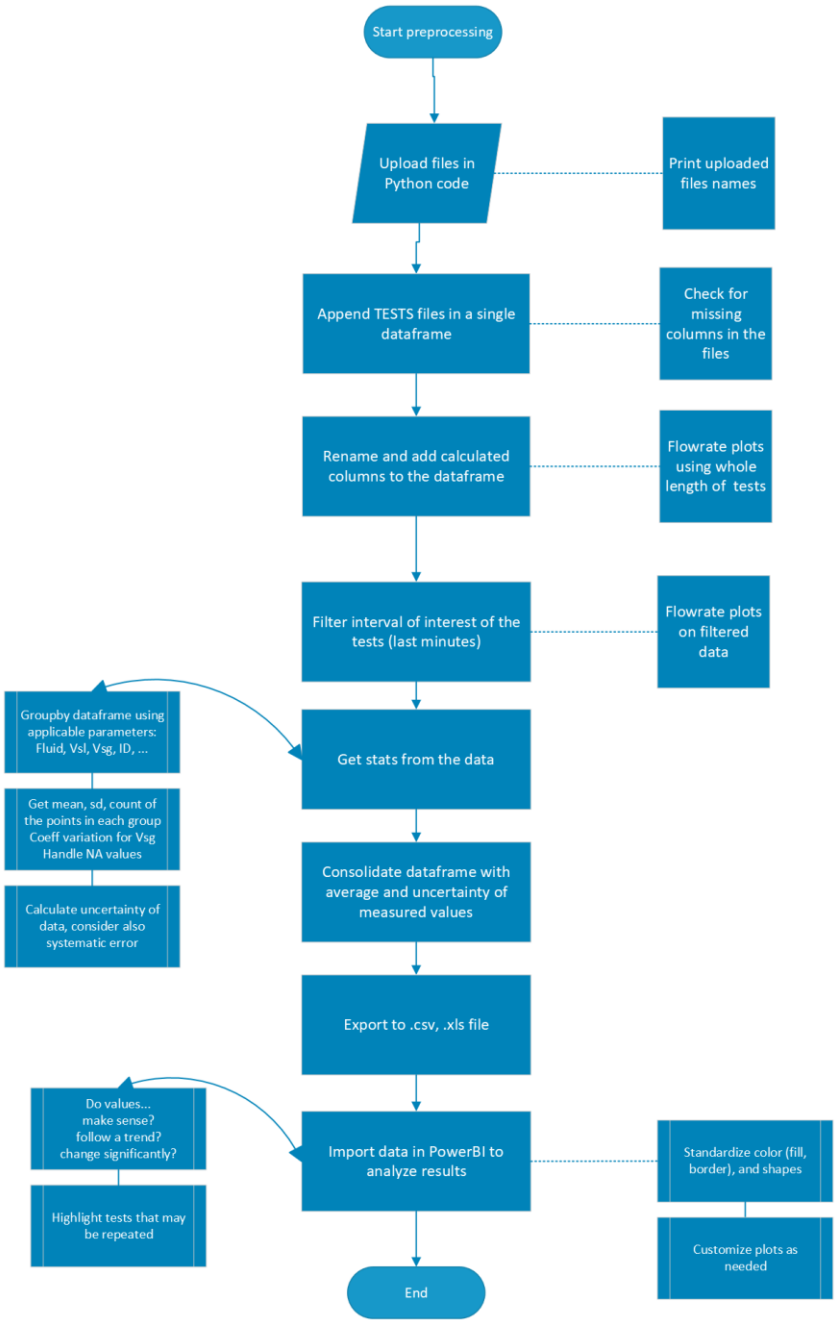

Figure 3.10 Flowchart of the code to pre-process data from the experiments

As mentioned before, the tests are monitored to ensure stable data acquisition and quality. Potential fluctuations in air flow rate must be considered, given the relevance of this parameter in the experiments. A PID algorithm is implemented in the LabVIEW program to regulate the control valve that allows air to flow into the test section. The aim is to match the desired superficial gas

velocity. Air density (ρ_A) is calculated by using the equation of state for an ideal gas, at a temperature *(T)* of 29 °C and the pressure *(P) at* the base of the test section. The specific constant for the gas (R_{air}) is calculated by dividing the universal gas constant (R) by its molar mass, which is 29 g/mol for air. This calculation is shown in Equation (3.1).

$$\rho_A = \frac{P}{R_{air}T} \qquad (3.1)$$

The superficial gas velocity (v_{Sg}) is determined by considering the measured mass flowrate ($\dot{m}$), the area of the pipe (A_p), and the air density, using Equation (3.2).

$$v_{Sg} = \frac{\dot{m}}{\rho_A A_p} \qquad (3.2)$$

A 10% margin of tolerance is used to ascertain the stability of the air flow, when comparing the desired and calculated velocities. The test must be run for no less than 3 continuous minutes in this stable state, otherwise it is not considered valid. Depending on the fluid rates, some tests were extended for up to 40 minutes to achieve this stability. Tests for which the ratio of mean and standard deviation (signal-to-noise ratio), was below 15 were repeated. This threshold value was chosen after running several tests and comparing results with those reported in similar studies.

Superficial gas velocity fluctuations are shown in Figure 3.11 for the last few minutes, when steady state is achieved. These fluctuations correspond to the tests without inserts and with a v_{SL} value of 0.00167 m/s and varying v_{Sg} values. Appendix A includes the velocity fluctuation plots for tests using inserts. The x-axis on the figures is backwards as it corresponds to the time left before operating the QCV's to finish the tests.

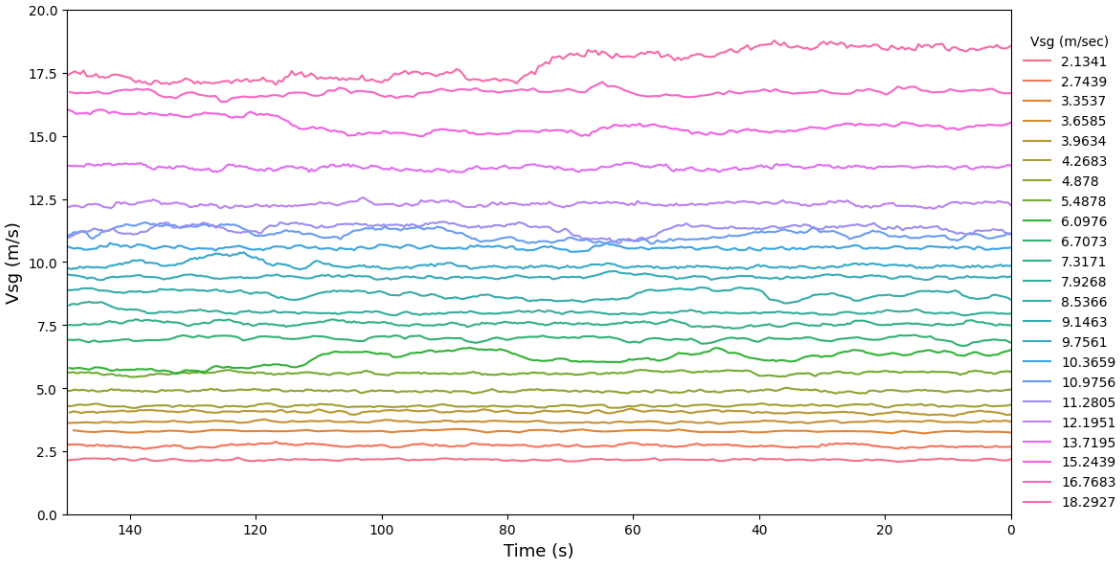

Figure 3.11 Air flowrate fluctuations for tests without inserts at v_{SL} 0.00167 m/s

Figure 3.12 shows a comparison of the set and actual superficial gas velocities for various tests. The data points indicate that the gas flowrate was properly controlled for all cases.

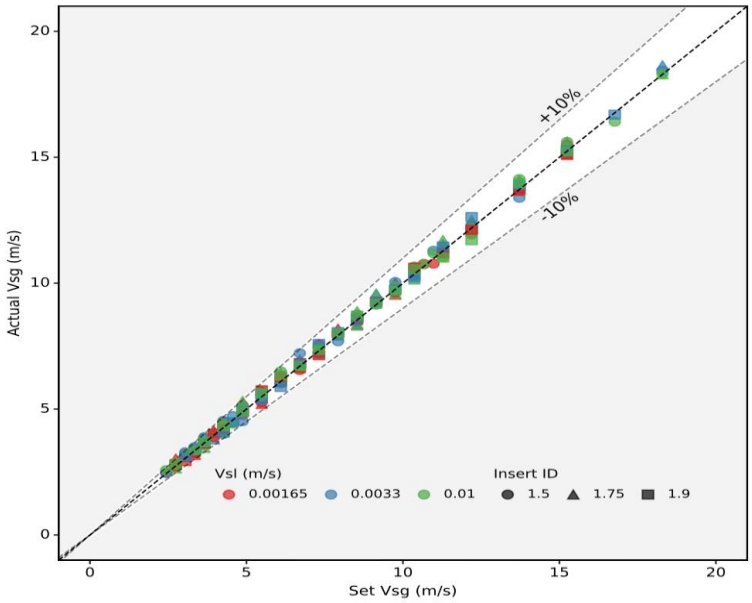

Figure 3.12 Actual vs set superficial gas velocity for various tests

The pressure data considered for further analysis correspond to the ones in the stable flow region, as presented above. To calculate the pressure gradient in the test section, the pressure

difference between the bottom PT and top PT is divided by the distance between them. The readings from various DPs are also used to obtain the pressure gradient by dividing the pressure readings over their corresponding lengths. The results obtained by these methods are similar, as observed in Figure 3.13. It is determined to use the results obtained using DP2 since it covers the longest section with a single instrument.

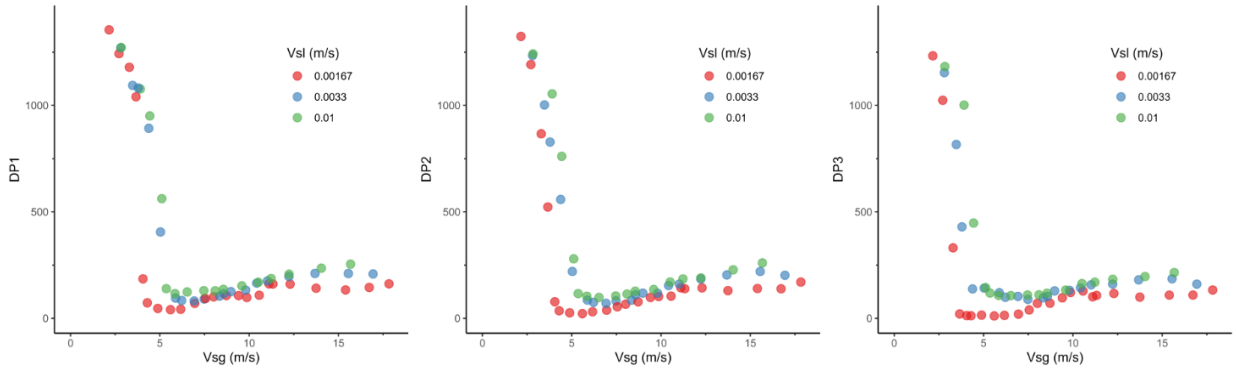

Figure 3.13 Comparison of values measured with various DP installed along test section

Liquid holdup (H_L) corresponds to the proportion of the pipe volume filled with liquid. At the end of each test, the liquid level (h_L) is determined using a tape affixed to the test section. The total length (h_{total}) of test section is 7.6 m (25 ft). Since the diameter of the test section is constant, Equation (3.3) serves to calculate the liquid holdup.

$$H_L = \frac{h_L}{h_{Total}} \qquad (3.3)$$

Figure 3.14 shows a schematic with the components required to determine the liquid holdup from the experimental tests, along with the actual snapshot of a measured liquid level.

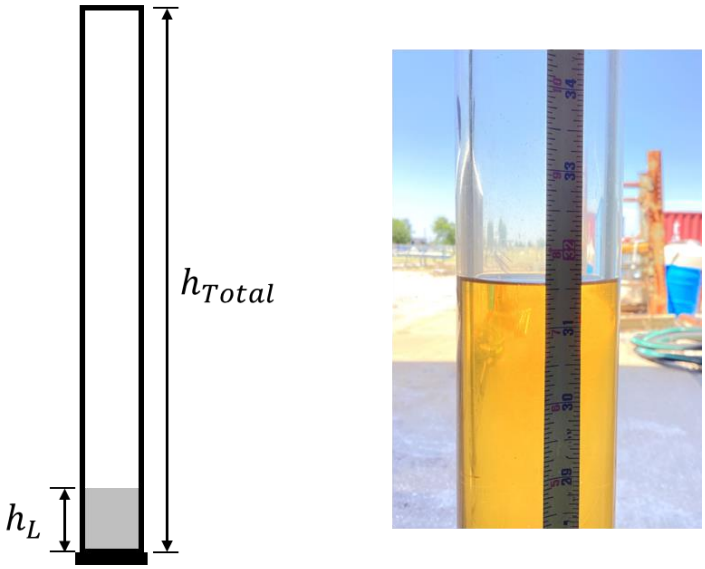

Figure 3.14 a) Schematic of liquid holdup determination b) Liquid level measured after a test

The test facility was previously benchmarked in a study by Alsanea et al. (2022), showing alignment with the data from other institutions. Therefore, a limited set of data was collected and compared with Alsanea's data to ensure reliability of the results.

3.5. Test matrix

This study employs a structured experimental matrix in which four key parameters are systematically varied to represent a range of operational scenarios. Table 3.2 shows the designed test matrix of the current study. Three superficial liquid velocities are considered along with up to 20 superficial gas velocities, enabling the simulation of varying production conditions. Said conditions include annular, churn and slug flow patterns. Previous investigations (Alsanea, 2018; Alsanea et al., 2023; Barreto et al., 2017; Skopich et al., 2015) on liquid loading reported the use of similar testing flowrate conditions. This study also includes v_{SL}=0.00167 m/s, not tested by

previous studies. This v_{SL} value is relevant to understanding the optimum range of conditions for the implementation of inserts in low liquid loading gas wells.

Some tests are run in the absence of inserts to obtain baseline data allowing comparison of the effects of inserts. The insert size is selected based on the common tool joint diameter reductions and available data for comparison. The sizes of tool joints are between 75% and 95% of the internal diameter of the tubing, which is 2" for the present study.

Table 3.2 Test matrix

Parameter	**Values**
Insert ID	1.5", 1.75", 1.9", *No insert (2")*
v_{SL}	0.00167, 0.0033, 0.01 m/s
v_{Sg}	2.4 – 18.3 m/s (8 – 60 ft/s)
Insert locations	Bottom (1), Bottom and Top (13), *No insert (0)*

In some cases, tests with identical conditions were repeated to ensure consistency, and the reported results are the averages of these repetitions. Additionally, a higher number of tests were conducted under certain circumstances. When significant variations were observed in the response variables, specifically pressure drop and liquid holdup, conducting more tests allowed for a finer level of data granularity. Also, additional tests were used to explore various combinations of parameters to identify optimal conditions for the implementation of inserts.

Alsanea (2022) evaluated the use of three inserts installed along the same experimental test section, identifying an opportunity for the use of inserts to address liquid loading issues. The present study aims to better understand the locality of the effects provided by the inserts to determine conditions that favor their implementation. Therefore, the tests conducted involve inserts installed at either one (1) or two locations (13).

Figure 3.15 illustrates various combinations of input parameters involved in this study for the multiphase flow tests. The x-axis includes the three tested liquid rate values represented through v_{SL}, while the y-axis corresponds to the set v_{Sg} values tested. Dots on the plot represent data points, where dot filling colors indicate the insert ID used, and their border colors correspond to the insert locations, as specified in Table 3.2. The cases where Insert ID is noted as 0 correspond to the tests where inserts were not used, and so no locations are assigned.

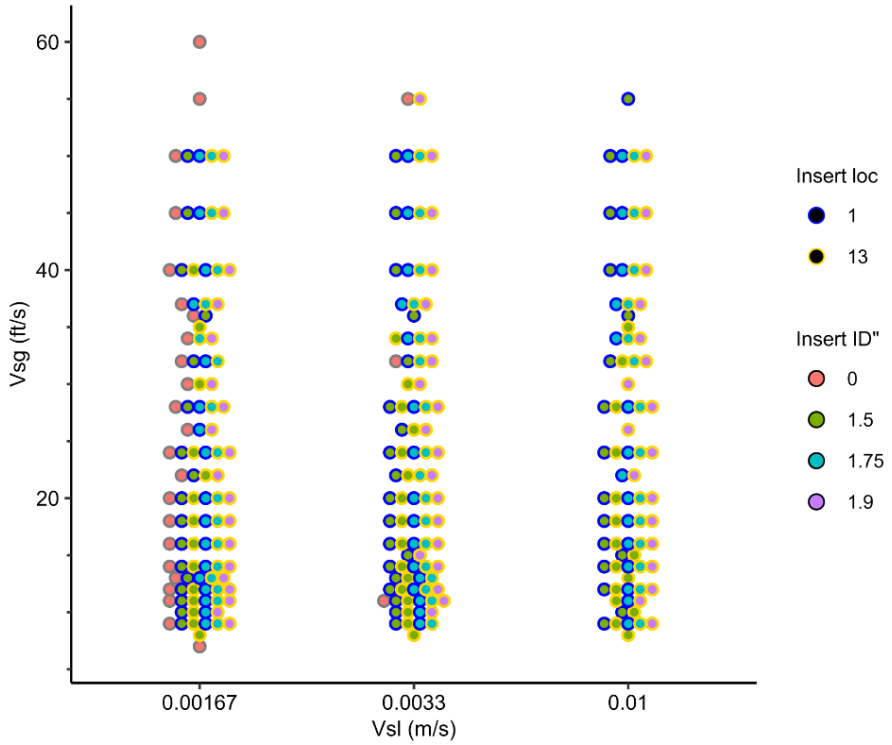

Figure 3.15 Summary of the tested experimental conditions

CHAPTER 4. TWO-PHASE FLOW EXPERIMENTAL RESULTS

This chapter presents the results of the experiments outlined in the previous chapter. The tests were conducted in a facility simulating a natural gas well with a 2 in ID vertical pipe at low liquid loading conditions. Partial tubing restrictions were simulated by insert rings, installed in up to 2 locations to prevent liquid film fallback and promote droplet entrainment. Three superficial liquid velocities were tested with superficial gas velocities ranging from 7 to 60 ft/s. Pressure drop and liquid holdup measurements, along with video recordings were collected for each test.

Uncertainty propagation calculations are represented in the plots using error bars. These error bars encompass instrumentation precision and statistical measures, A more detailed description of these calculations can be found in the work by Alsanea (2022).

There are two sections in this chapter. The first one corresponds to the tests without inserts, serving as the baseline scenario and used to evaluate the performances of various flow models. The second and main section corresponds to the tests in which inserts were installed. The aim is to evaluate various combinations of parameters that would yield a positive net effect on flow.

4.1. Testing Results Without Inserts

The first step to understand the effect of inserts on liquid loading in vertical tubulars is to characterize the problem itself. For this purpose, baseline tests were conducted at varying v_{SL} and v_{Sg} conditions without inserts.

4.1.1. Flow behavior – Visual observations

Figure 4.1 displays the flow behavior for the tests without inserts at a fixed v_{SL} of 0.00167 m/s, and three values of v_{Sg}. Different flow patterns are exhibited for each of the v_{Sg} cases. Figure 4.1 (a) depicts the flow behavior of the lowest tested v_{Sg}, characterized by a constant mixing of liquid and gas in a chaotic churn flow. Figure 4.1 (b) displays the middle gas rate, where liquid film fallback is present while droplets travel upwards in the gas core, in a churn-annular flow. In Figure 4.1 (c), annular flow is observed with a high v_{Sg} where droplets and liquid film move upwards continuously.

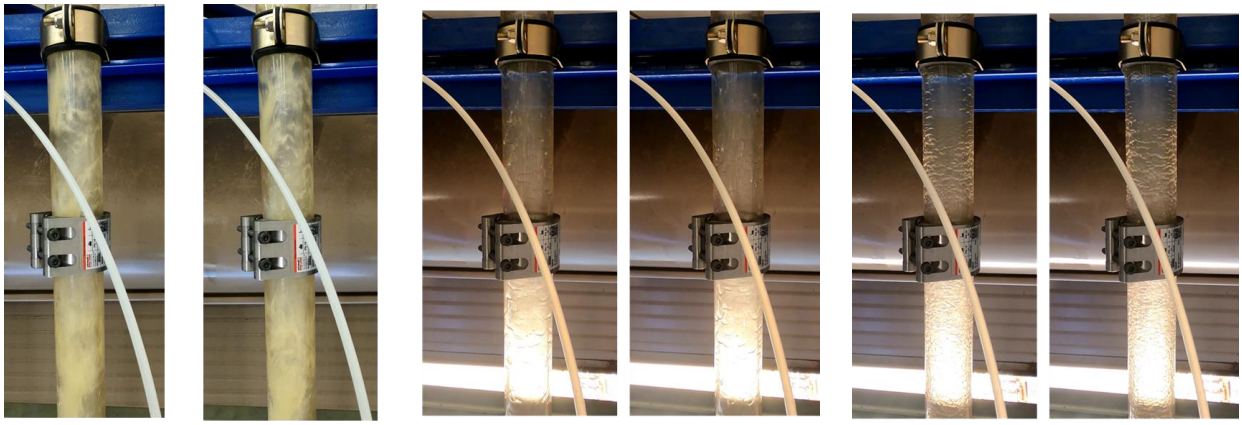

Figure 4.1 Two-phase flow behavior at v_{SL} of 0.00167 m/s without inserts - effect of v_{Sg}

The critical gas velocity corresponds to the v_{Sg} at which the onset of liquid loading takes place. As discussed in CHAPTER 2, multiple experimental investigations conclude that liquid film reversal defines this onset. From visual observations, it was determined that the critical gas velocity is v_{Sg} =9.38 m/s (30.8 ft/s) at v_{SL}= 0.00167 m/s in the absence of inserts.

4.1.2. Measured parameters – Pressure drop and liquid holdup

Figure 4.2 illustrates the relation of superficial gas velocity with pressure drop (left) and liquid holdup (right) at the lowest liquid rate, v_{SL} =0.00167, in the absence of inserts. Two flow patterns are identified from the visual observations and marked with circles for annular flow and triangles for churn flow.

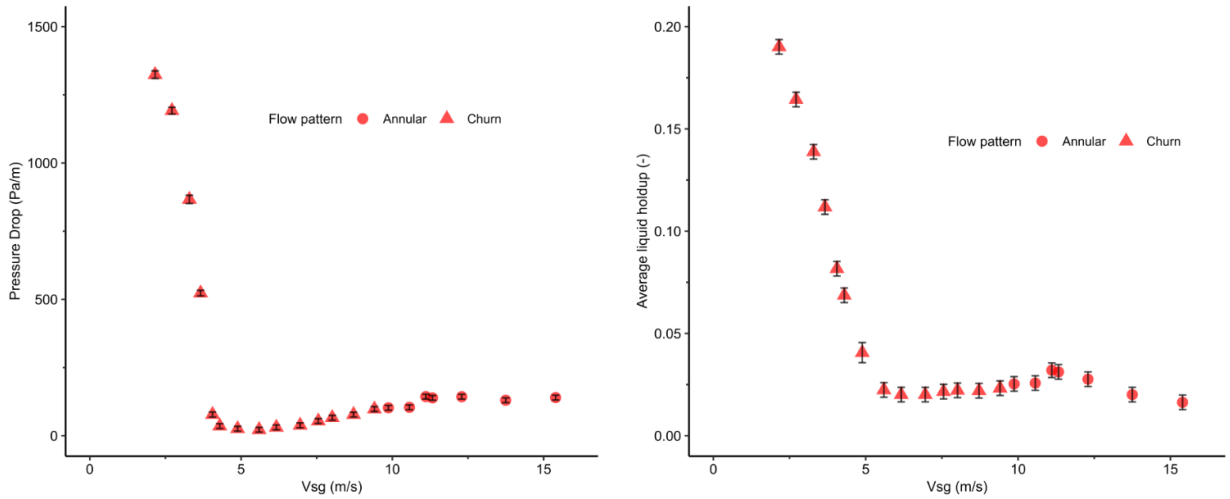

Figure 4.2 Pressure drop and liquid holdup vs superficial gas velocity at v_{SL} = 0.00167 m/s

Figure 4.2 shows that $v_{Sg,min}$= 5.6 m/s corresponds to the minimum pressure drop. As the v_{Sg} decreases below this value, $\left(\frac{dP}{dL}\right)_T$ rises significatively. On the other hand, for $v_{Sg} > v_{Sg,min}$, the total pressure drop continually increases in a smooth manner by increasing the v_{Sg}. The liquid holdup changes in a similar manner to pressure drop, with a local minimum H_L found at v_{Sg}=6.1 m/s. This suggests that the liquid holdup (H_L) is associated with the total pressure drop, in particular with the sharp increase at $v_{Sg} < v_{Sg,min}$. This is due to the inability of the gas to unload the well at these low gas rates, which results in liquid accumulation imposing an extra pressure drop. On the other hand, the liquid holdup initially has a small increase and then starts reducing for v_{Sg}

> $v_{Sg,min}$. The transition from annular to churn flow takes place at a v_{Sg} higher than both $v_{Sg,min}$ and the local minimum for H_L.

Figure 4.3 displays a breakdown of the total pressure drop $\left(\frac{dP}{dL}\right)_T$ into its components. Frictional pressure drop $\left(\frac{dP}{dL}\right)_f$ is shown using purple square markers and gravitational term is displayed using yellow circles. At low v_{Sg} values, the gravitational term $\left(\frac{dP}{dL}\right)_G$, associated with liquid holdup, is the main source of pressure drop. Then as v_{Sg} increases, the gravitational term loses significance and the frictional term $\left(\frac{dP}{dL}\right)_f$ gains more relevance. The negative value of the frictional pressure drop at low v_{Sg} is an indicator of liquid film reversal in these cases. The v_{Sg} value where the frictional term changes from positive to negative was considered as the onset of liquid loading by Alsanea (2022). This point happens at a v_{Sg} of 13.5 m/s for the tested v_{SL}.

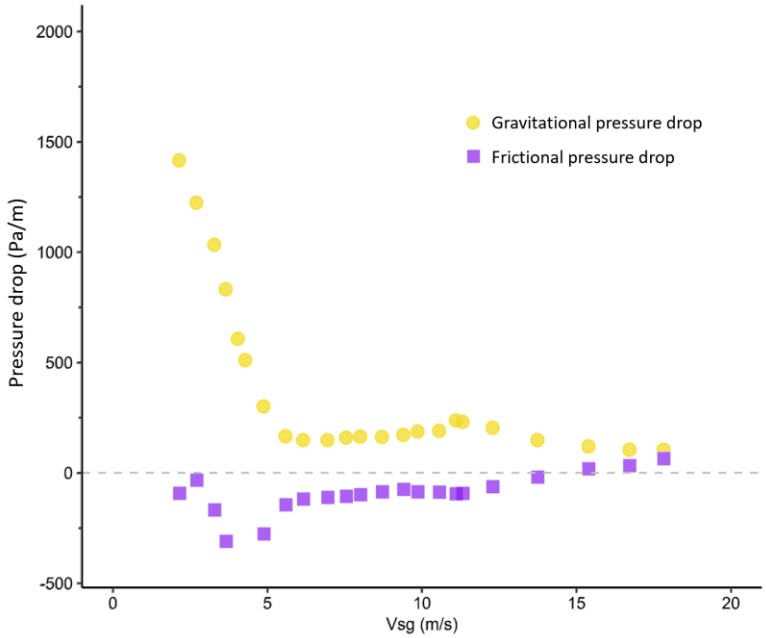

Figure 4.3 Frictional and gravitational pressure drop vs v_{Sg} at v_{SL} = 0.00167 m/s

Figure 4.4 focuses on the frictional component of pressure, $\left(\frac{dP}{dL}\right)_f$. The flow patterns identified are shown with different markers. The sharp increase observed after the transition to annular flow suggests that the frictional losses dominate the pressure drop at higher gas rates as reported in the literature.

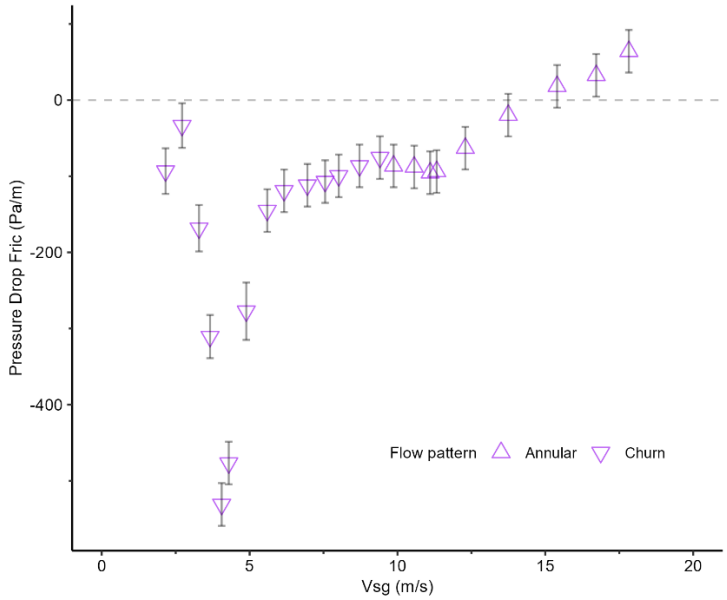

Figure 4.4 Frictional pressure drop vs superficial gas velocity at v_{SL} = 0.00167 m/s

4.2. Test Results with Inserts

Putra and Christiansen (2001) suggested that inserts boost liquid lifting by preventing liquid fallback and enhancing droplet generation. These phenomena were later documented by other authors as discussed in CHAPTER 2. Some of the results from the current study and discussed in the following section were presented at a recent conference (Mateus-Rubiano et al., 2023). Alsanea (2022) discussed that a wave growth region develops above the insert, and the gas core ruptures the liquid bridge, leading to an increase in droplet entrainment, shown in Figure 4.5.

The tests in which inserts were installed along the test section will be discussed below. The effects of inserts on pressure drop, liquid holdup, and flow behavior are analyzed for various combinations of insert sizes and locations. Snapshots of the recordings are first presented to depict the impact on flow behavior before analyzing the measured variables.

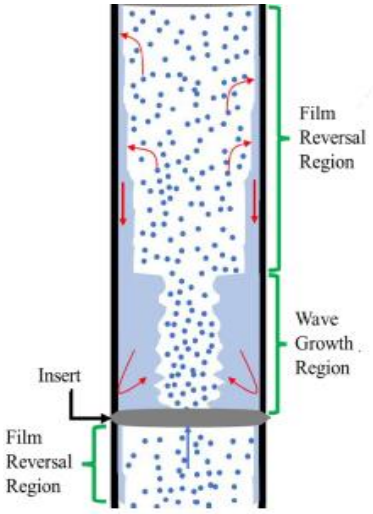

Figure 4.5 Flow behavior with insert in test section (Alsanea, 2022)

4.2.1. Flow behavior – Visual observations

To facilitate the comparison of the observed flow behaviors, the following snapshots correspond to recordings of the camera located at the top section of the facility. Also, unless otherwise noted, the tests shown were conducted with two inserts located in positions 1 and 3 (bottom and top), from Figure 3.2.

Figure 4.6 depicts the two-phase flow behavior at v_{SL} = 0.00167 m/s and various v_{Sg} values, in presence of inserts with the ID of 1.75”. The restrictions have an immediate impact on the flow. Two distinct behaviors are observed before and after them. The upward flowing liquid collides with the inserts generating droplets. Also, liquid waves of high amplitude are found after the inserts aiding to carry the liquid film upward.

A comparison with Figure 4.1, where the same liquid and gas flowrates are tested without inserts, highlights that the flow preceding the insert may be affected by its presence. Also, it is observed that the impact of the inserts on flow behavior is influenced by the v_{Sg}. Figure 4.6 (a) depicts the flow behavior at the lowest v_{Sg}. In this case, a churn flow behavior is observed, yet most of the liquid is now concentrated above the insert, while a thin liquid film is falling downward on the pipe wall. Figure 4.6 (b) corresponds to a slightly higher gas rate. A clear difference is observed in the liquid distribution between this case and the test without insert shown in Figure 4.1 (b). This case displays the wave growth region previously discussed, while the test without inserts shows droplets traveling upward in the gas core but a higher liquid amount falling downward on the pipe wall. Figure 4.6 (c) visualizes the highest gas flow rate. This annular flow behavior is minimally affected by the presence of inserts. Only a minor disruption can be detected when looking in detail above the insert, while no differences are observed underneath it.

Figure 4.6 Two-phase flow behavior at v_{SL} = 0.00167 m/s with 1.75 in insert ID - effect of v_{Sg}

In short, the biggest effect of inserts on flow behavior occurs at middle to low v_{Sg} values where churn flow pattern is observed. At high v_{Sg}, where annular flow takes place, no significant differences are visually identified in the flow.

Figure 4.7 depicts the two-phase flow behavior at v_{Sg} = 4.26 m/s (14 ft/s) and various v_{SL} values, in presence of inserts with an ID of 1.75". Figure 4.7 (a) exhibits the lowest v_{SL} and resembles Figure 4.6 (b) with a slightly different gas rate. Figure 4.7 (b) and Figure 4.7 (c) correspond to the middle and highest tested v_{SL} values. As expected, when v_{SL} increases, the amount of liquid both in the wave growth region above the insert and in the downward falling film below the insert increases as well, leading to a more chaotic flow. Changes in the v_{SL}, even by orders of magnitude smaller than v_{Sg} variations can have significant impacts on the flow pattern.

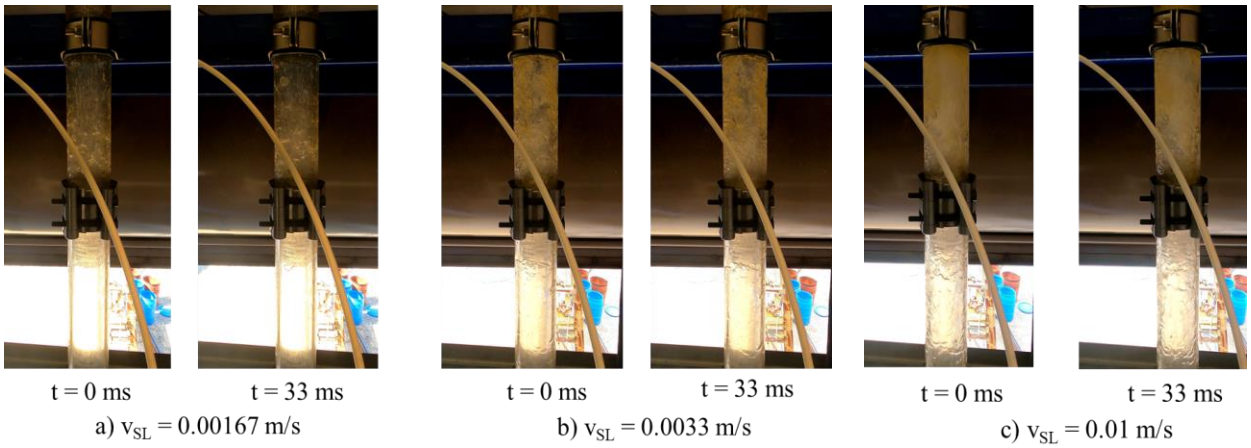

Figure 4.7 Two-phase flow behavior at v_{Sg} = 14 ft/s (4.26 m/s) with insert ID 1.75" - effect of v_{SL}

Figure 4.8 depicts the two-phase flow behavior at v_{Sg} = 3.66 m/s (12 ft/s) and v_{SL} = 0.0033 m/s, in presence of inserts with different sizes. Inserts with smaller ID seem to lift a greater amount of liquid above them. Figure 4.8 (a) corresponds to the tests using 1.5" ID inserts, providing the largest restriction to the flow. Figure 4.8 (b) shows a test with intermediate insert opening, 1.75" ID. This one is allowing more liquid to fall downward below the insert on the pipe wall. In Figure 4.8 (c) a 1.9" ID insert is used, providing the least restriction of the three cases. It shows the largest amount of liquid flowing downward on the pipe wall below the insert.

The observed results in Figure 4.8, regarding the amount of fluid flowing downwards below the insert, agree with the measured data. The liquid holdup (H_L) obtained for various insert ID's is as follows: 0.078 for 1.5", 0.111 for 1.75", and 0.115 for 1.9".

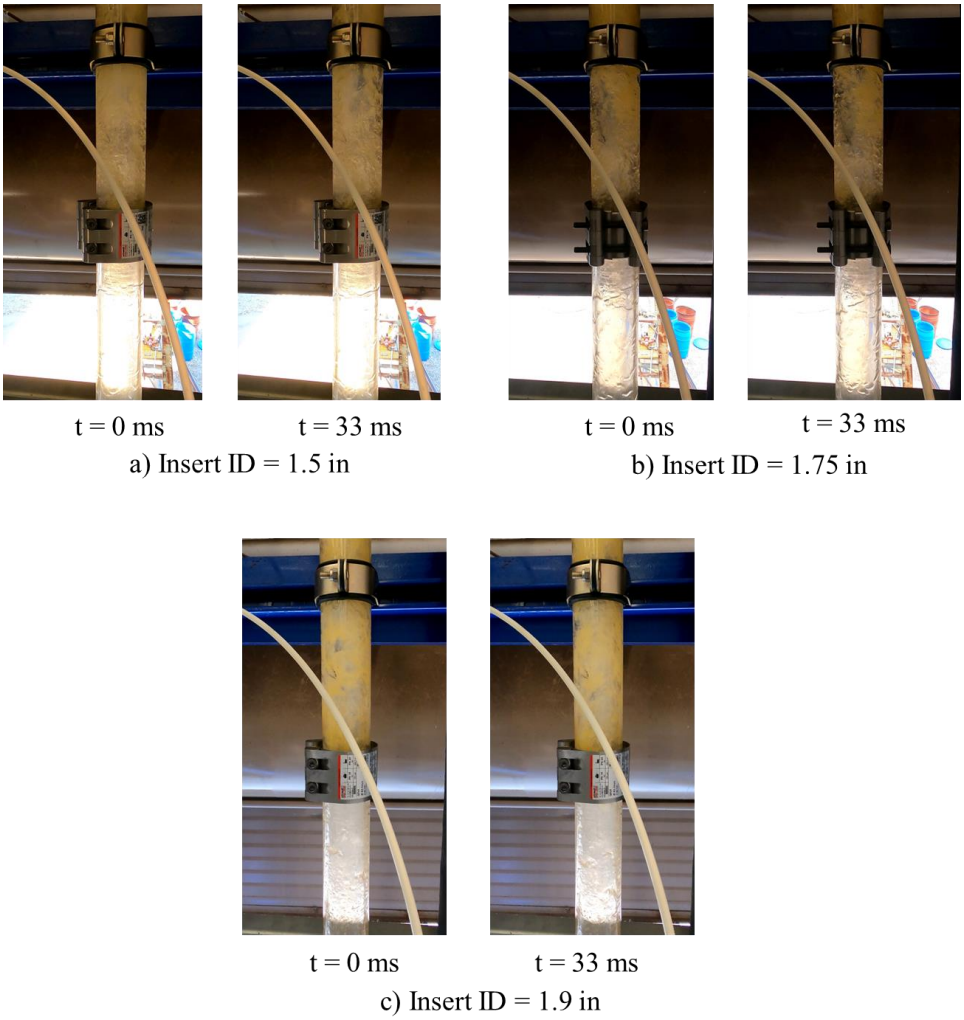

Figure 4.8 Two-phase flow behavior at v_{SL} = 0.0033 m/s and v_{Sg} = 12 ft/s (3.66 m/s) - effect of insert ID

The impacts of operational parameters such as v_{Sg} and v_{SL} on the flow pattern were discussed previously. The effect of insert size on the flow depends on the flow characteristics in which it is used. Figure 4.9 depicts the two-phase flow behavior at v_{Sg} = 8.54 m/s (28 ft/s) and v_{SL} = 0.0033 m/s, in presence of inserts with different ID's. In contrast with Figure 4.8 for which liquid

and gas rate conditions yielded a chaotic churn flow, in Figure 4.9 the fluid behavior is closer to the transition to annular flow. The falling liquid film on the pipe wall below the insert looks similar for the three insert sizes. This is consistent with the similar H_L data yielded for the three tests, which are as follows: 0.026 for 1.5", 0.025 for 1.75", and 0.026 for 1.9". Considering the uncertainty associated with these measurements, the data are not significantly different. Therefore, it is suggested that the impact of the insert ID size on the flow behavior and liquid holdup is more significant at low v_{Sg} values, around the churn flow region. Conversely, at higher v_{Sg} values, approaching annular flow, the effect of insert ID size diminishes.

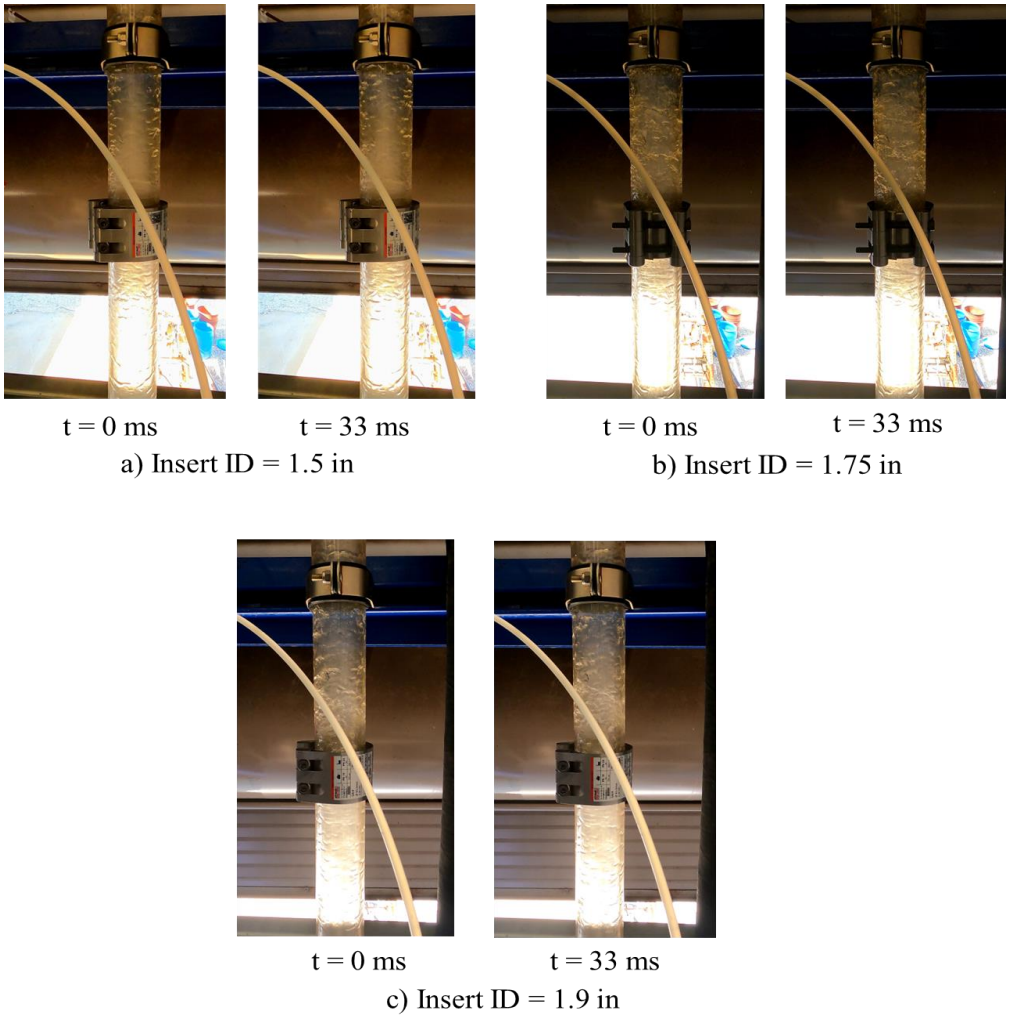

Figure 4.9 Two-phase flow behavior at v_{SL} = 0.0033 m/s and v_{Sg} = 28 ft/s (8.54 m/s) - effect of insert ID

The flow experiments shown in the previous figures involved the use of inserts in two locations, location 1 and 3 (bottom and top) of the test section. Figure 4.10 exhibits the view of the bottom and top section cameras, for a test in which a single insert is present in the test section and located at the bottom (location 1). The waves generated after the insert, shown in Figure 4.10 (a) are mostly dissipated before reaching the top of the test section, shown in Figure 4.10 (b).

Figure 4.10 Two-phase flow behavior at v_{SL} = 0.00167 m/s and v_{Sg} = 12 ft/s, 1.5" ID insert at location 1 (bottom)

Figure 4.11 depicts the two-phase flow behavior at v_{Sg} = 3.66 m/s (12 ft/s) and v_{SL} = 0.00167 m/s, for tests with different numbers of 1.5" ID inserts installed. Figure 4.11 (a) corresponds to the case without inserts. A continuous liquid film is observed falling back on the pipe wall, while droplets travel upwards in the gas core. Figure 4.11 (b) corresponds to the case where an insert is located at the bottom of the test section. In here, liquid film is falling back but at a slower rate than the one without inserts. In Figure 4.11 (c) two inserts are installed, at locations 1 and 3, and the amount of liquid falling back seems to be even lower.

As discussed earlier for the insert size, other operational conditions such as the gas and liquid rate may impact the significance of a parameter. It is likely that at higher gas rates, leading to annular flow pattern, the visual distinctions of flow behavior become less apparent. However, other output parameters such as pressure drop may still exhibit noticeable variations.

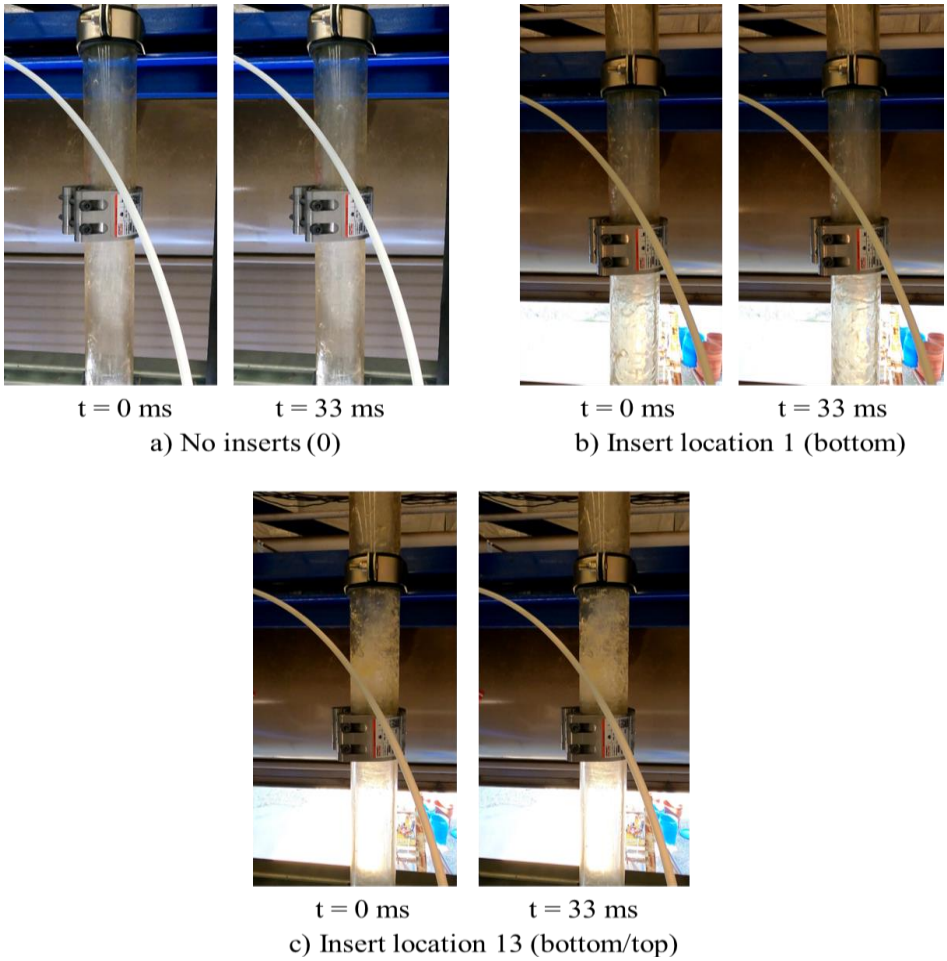

Figure 4.11 Two-phase flow behavior at v_{SL} = 0.00167 m/s and v_{Sg} = 12 ft/s, 1.5" ID – effect of insert location

4.2.2. Pressure drop and liquid holdup – Insert effects

The remainder of Section 4.2 looks at the results of the tests with inserts from a quantitative perspective. The baseline tests discussed in Section 4.1 are used to assess the impact of insert implementation on liquid lifting performance. Certain plots may include more than 2 variables

with the purpose of examining their combined effects. This subsection is focused on tests with two inserts installed, at locations *1* and *3*, collectively referred to as *13*.

Some additional parameters were defined to better quantify the effects of inserts and show their significances. The pressure drop difference and liquid holdup difference were determined by subtracting the values obtained with inserts from those obtained without inserts (baseline scenario). These definitions are shown in Equation (4.1) and Equation (4.2).

$$\text{Pressure drop difference: } \left(\frac{dP}{dL}\right)_{T,diff} = \left(\frac{dP}{dL}\right)_{T,without\ inserts} - \left(\frac{dP}{dL}\right)_{T,with\ inserts} \quad (4.1)$$

$$\text{Liquid holdup difference: } \left(H_{L,diff}\right) = H_{L,without\ inserts} - H_{L,with\ inserts} \quad (4.2)$$

Positive values for these terms indicate reductions in the amount of liquid accumulated or in the pressure losses through the test section, both of which are favorable. Therefore, such positive values are associated with improvements in liquid unloading by the implementation of inserts.

Since the actual v_{Sg} values may fluctuate and slightly vary, a linear interpolation was used to determine the corresponding pressure drop and liquid holdup of the base scenario for each liquid rate. The calculated *difference* value was divided by the base case value and multiplied by 100% to obtain the relative percentage of changes, as shown in Equation (4.3) and Equation (4.4).

$$\text{Pressure drop relative change}(\%) = \frac{\text{Pressure drop difference}}{\text{Pressure drop without inserts}} \times 100 \quad (4.3)$$

$$\text{Liquid holdup relative change}(\%) = \frac{\text{Liquid holdup difference}}{\text{Liquid holdup without inserts}} \times 100 \quad (4.4)$$

Figure 4.12 illustrates the pressure drop data of the tests with two inserts at locations 1 and 3, and at various liquid rates coded by colors: red for 0.00167 m/s, blue for 0.0033 m/s and green for 0.01 m/s. Flow patterns are denoted using circle markers for annular flow and triangle markers

for churn flow as identified by visual observations. Figures (a), (b), and (c) correspond to the insert ID's of 1.5, 1.75, and 1.9 inches, respectively.

Experiments using 1.5" ID inserts, Figure 4.12 (a), yield greater pressure drop values in the annular flow region, than tests with larger insert ID's. This is explained by the greater flow restriction imposed by smaller ID inserts. For all cases, the annular-churn flow transition occurs at a v_{Sg} slightly higher than the $v_{Sg,min}$ value. Also, in all cases as v_{SL} increases, the pressure drop increases, as a result of higher liquid holdup values. At high v_{SL} cases, $v_{Sg,min}$ moves to higher v_{Sg} values at the right side of the plot, and the sharp increase in pressure drop begins at a higher v_{Sg}. This is associated with an earlier sharp increase in liquid holdup, resulted from the transition to churn-slug flow at higher v_{SL} cases.

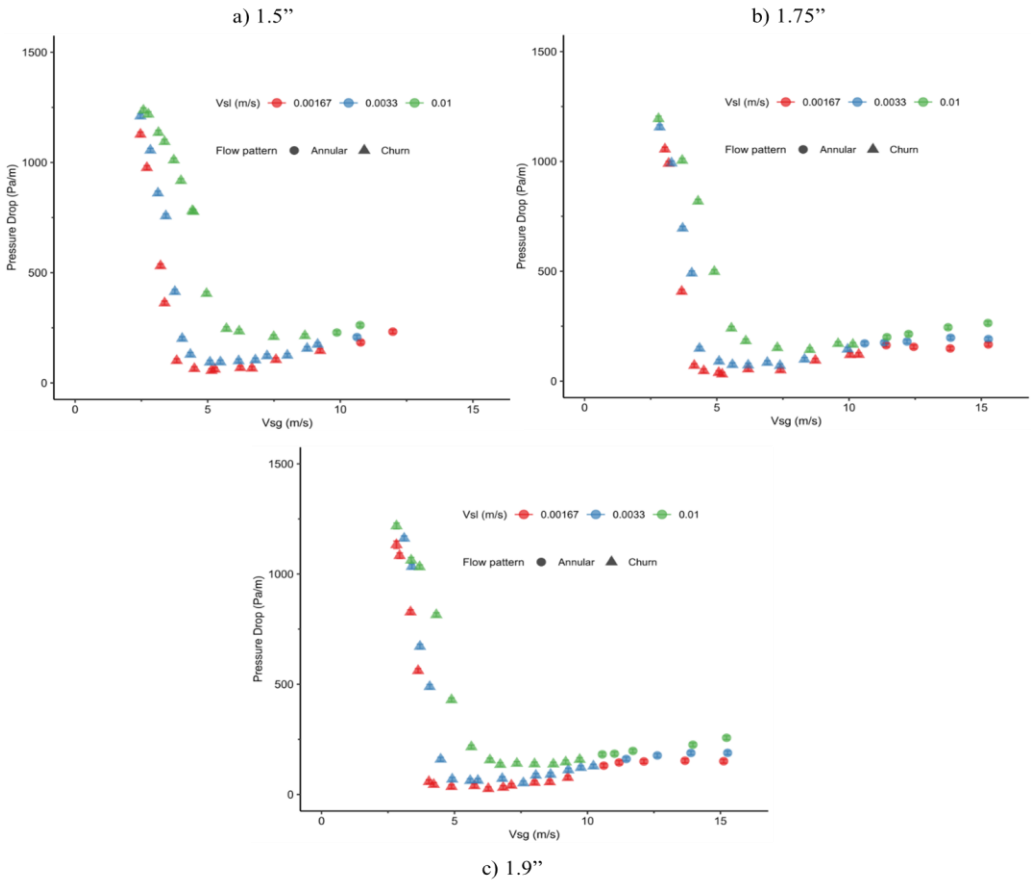

Figure 4.12 Total pressure drop vs v_{Sg} at various liquid rates. Inserts at locations 13

Figure 4.13 showcases a breakdown of $\left(\frac{dP}{dL}\right)_T$ into its components, $\left(\frac{dP}{dL}\right)_f$ and $\left(\frac{dP}{dL}\right)_G$. Frictional pressure drop is shown using square markers, while the gravitational term is displayed using diamond markers. Insert size (ID) is indicated using three colors: teal for 1.5", orange for 1.75", and purple for 1.9". The no-insert case is also included in red. The $\left(\frac{dP}{dL}\right)_G$ increases notably at higher v_{SL} values, while it decreases with increasing v_{Sg} values for all cases. The $\left(\frac{dP}{dL}\right)_f$ displays slight decreasing trends as the v_{Sg} drops for all cases, becoming negative with the liquid fallback.

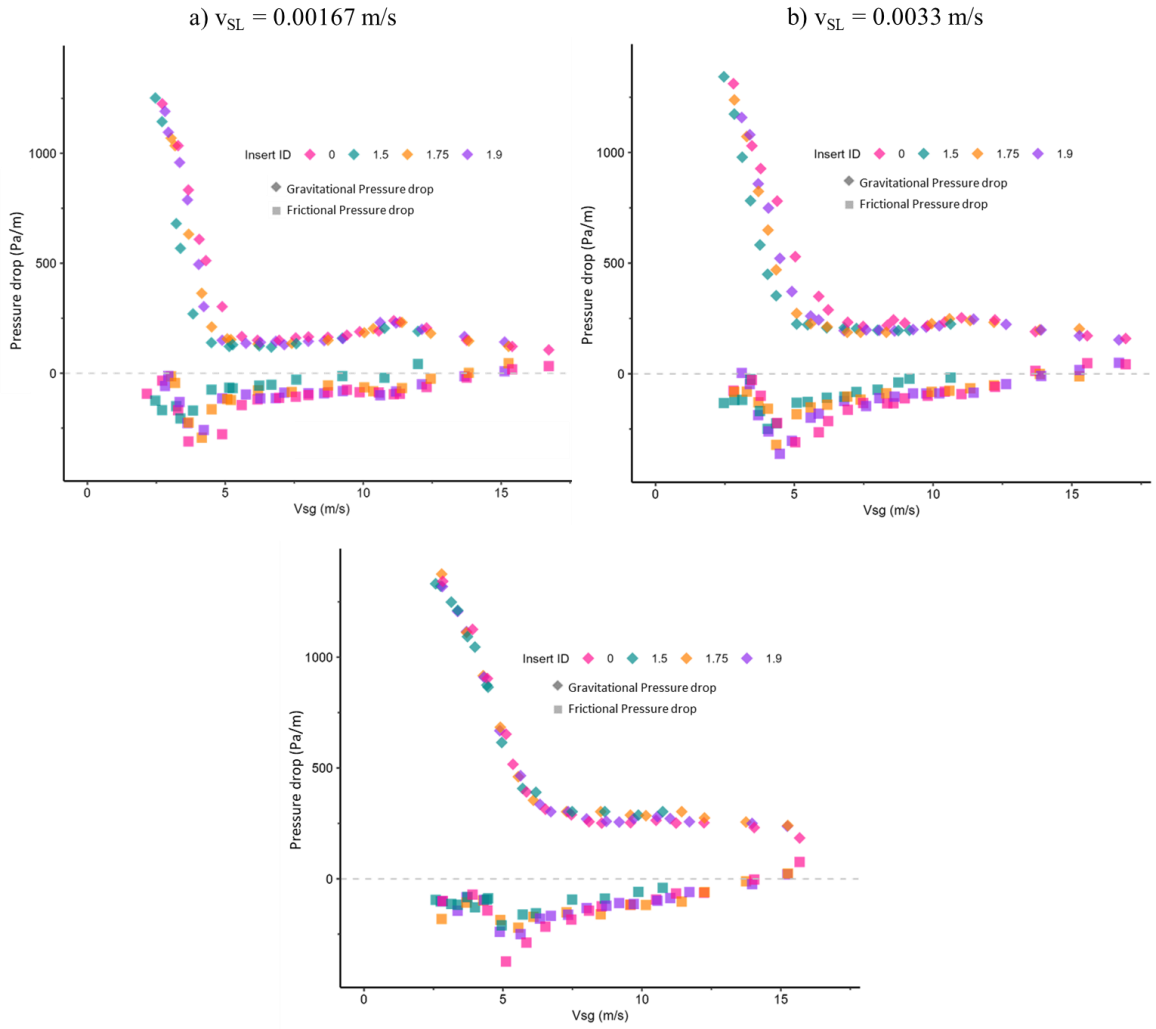

Figure 4.13 Frictional and gravitational pressure drop vs v_{Sg} for various insert ID's at locations 13

$\left(\frac{dP}{dL}\right)_G$ is impacted by insert ID in the churn flow region at low v_{Sg} and low v_{SL} values. This is observed when the markers previously overlapping in the annular flow at high gas rates, no longer coincide in the range $3<v_{Sg}<6$ m/s *A*s v_{Sg} increases, $\left(\frac{dP}{dL}\right)_G$ term loses importance and $\left(\frac{dP}{dL}\right)_f$ gains more relevance due to the increase of frictional losses.

The smallest insert ID, 1.5", consistently displays greater $\left(\frac{dP}{dL}\right)_f$ values, in particular when v_{Sg} increases in the annular flow region. This is explained by a greater insert restriction on the flow at higher gas rates. Also, this insert ID yields the lowest $\left(\frac{dP}{dL}\right)_G$ for v_{SL} values of 0.0033 and 0.00167 m/s in the churn flow region at v_{Sg} <5 m/s. At the highest v_{SL} of 0.01 m/s, $\left(\frac{dP}{dL}\right)_G$ is not affected by insert ID. This shows that the insert effects are more pronounced at lower liquid rates.

Figure 4.14 presents the pressure drop difference between tests with various insert sizes and the baseline case with no inserts. The values are calculated using Equation (4.1). As previously mentioned, positive difference values translates into positive insert effects. At the lowest liquid rate, with the v_{SL} of 0.00167 m/s, there are noticeable improvements for the smallest insert diameter (1.5") at v_{Sg} < 4 m/s, while the outcomes vary for the other sizes. At v_{SL}=0.0033 m/s, the best results are obtained with v_{Sg} values up to 5 m/s for all insert sizes. For the highest liquid rate, v_{SL} = 0.01 m/s, there is virtually no improvement in pressure drop from the use of inserts, as the baseline scenario consistently yields lower pressure drop values than the cases with inserts.

The insert effect on pressure drop becomes negative at the high gas rates of annular flow for all the tested liquid rates, due to the added friction. This effect also becomes negligible at the lowest gas rates, when approaching slug flow. The inserts seem to be the most effective within the churn flow region.

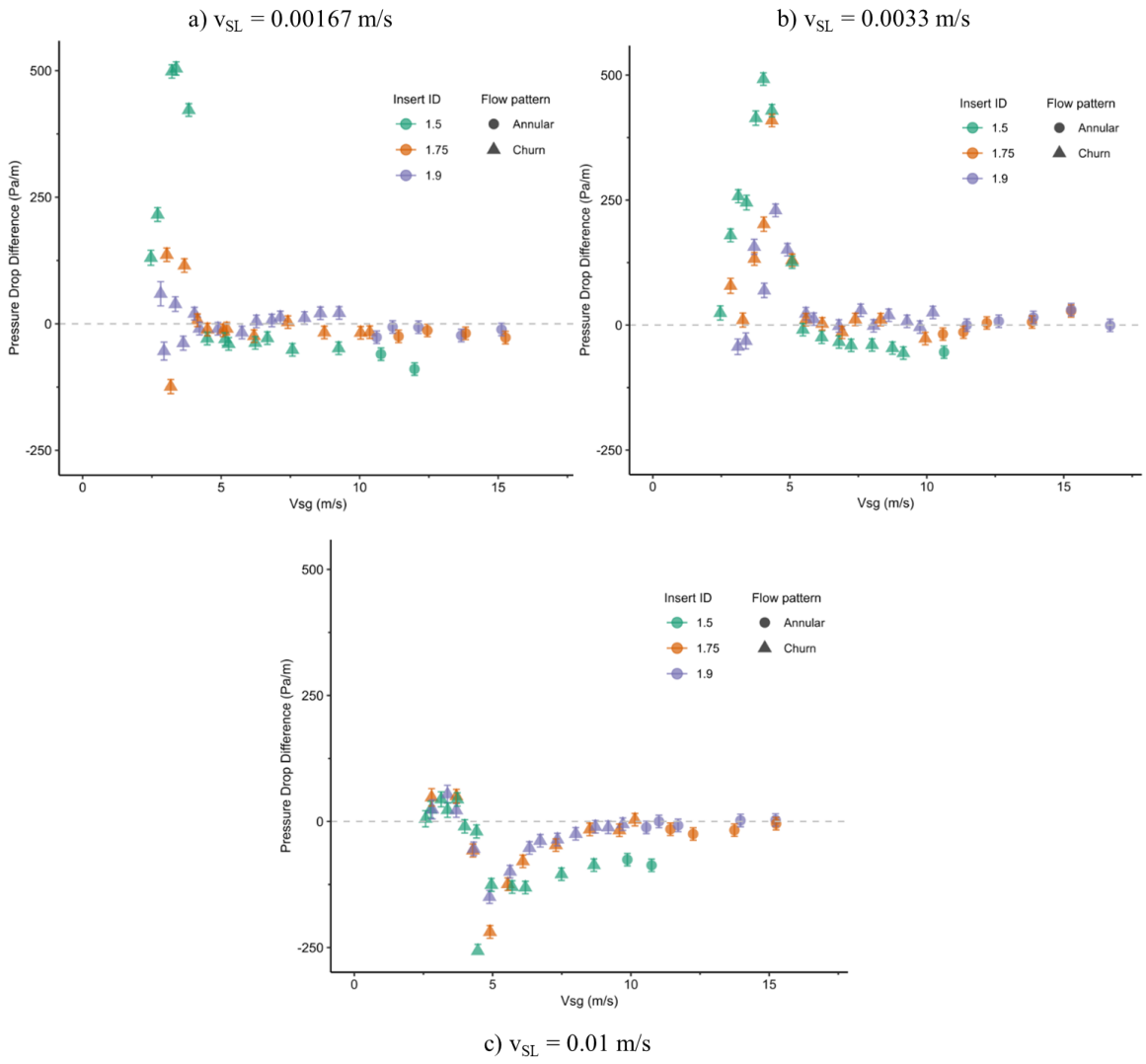

Figure 4.14 Pressure drop difference vs v_{Sg} with various insert ID. Inserts location 13

Figure 4.15 illustrates the liquid holdup data of the tests with inserts at locations 13 at various v_{SL} values coded by color. Flow patterns are identified with different markers. Each subfigure corresponds to a different insert size. As expected, higher v_{SL} results in higher liquid holdup (H_L) values for all the cases. At v_{Sg} values greater than the local minimum H_L, around v_{Sg} = 6 m/s, the insert ID no longer impacts H_L in a significant manner. Also, a peak with a local maximum H_L seems to coincide with the annular to churn flow pattern transition identified visually during the tests. This peak becomes more noticeable as v_{SL} gets smaller.

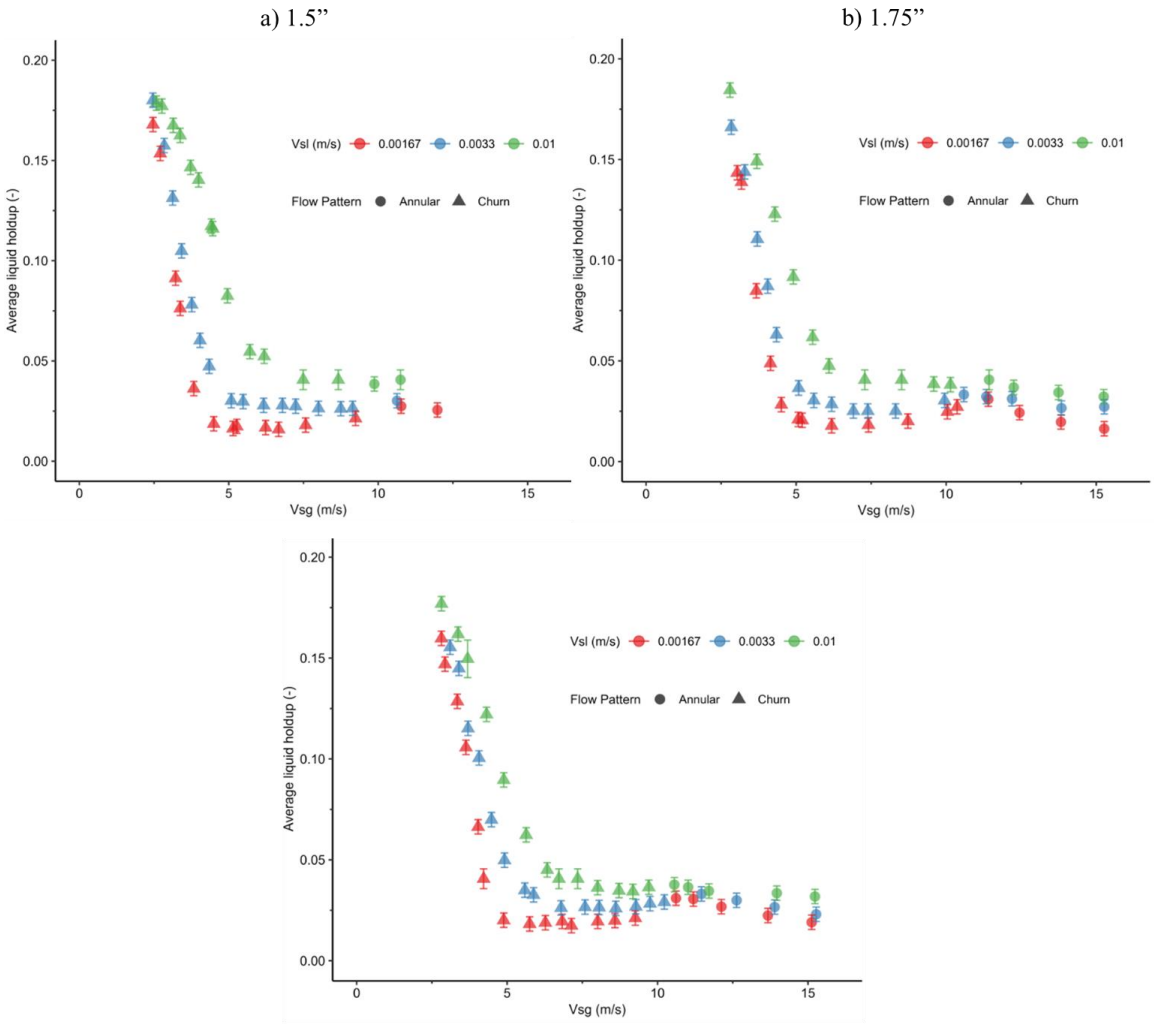

Figure 4.15 Liquid holdup vs v_{Sg} at various liquid rates with inserts at locations 13

Figure 4.16 details the H_L for the tests with inserts at locations 13 in churn flow at v_{Sg} <10 m/s. The v_{SL} is identified with the marker shapes circle, triangle, and square for 0.00167, 0.0033, and 0.01 m/s, respectively. Inserts ID’s are distinguished by different colors. Three trends can be readily identified in the plot. Higher v_{SL} values consistently yield greater liquid holdups. Square markers with different colors overlap, indicating that the insert size has no effect on the liquid holdup for the highest v_{SL}, 0.01 m/s. On the other hand, in the v_{Sg} range of 3-5 m/s, the triangles

and the circles of different colors do not overlap. This indicates that the insert ID is influencing H_L at low v_{SL} values, before the transition to slug flow.

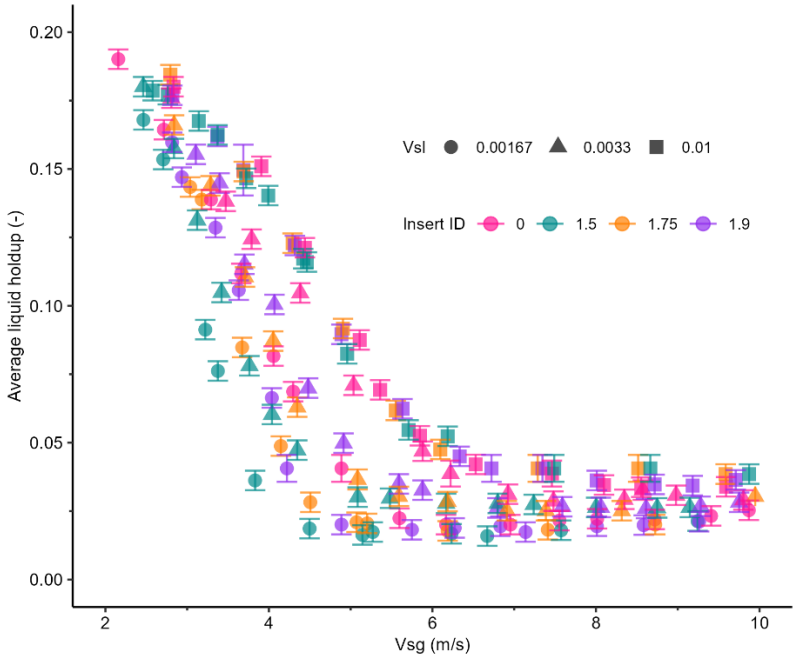

Figure 4.16 Liquid holdup vs v_{Sg} with inserts at two locations in churn flow.

Figure 4.17 presents the liquid holdup difference between tests with various insert sizes and the baseline scenario, with no inserts. The values are calculated using Equation (4.2). The inserts provide the most significant improvement in liquid holdup within the churn flow region with $3<v_{Sg}<6$ m/s and for the lower liquid rates. Within this region, the 1.9" insert ID has the smallest positive effect. In short, the test results reveal that when two inserts are used their internal diameter plays a role on its effectiveness and the favorable v_{Sg} range for its implementation. The insert effects are mostly positive for the lower liquid rates and in the v_{Sg} range corresponding to churn flow.

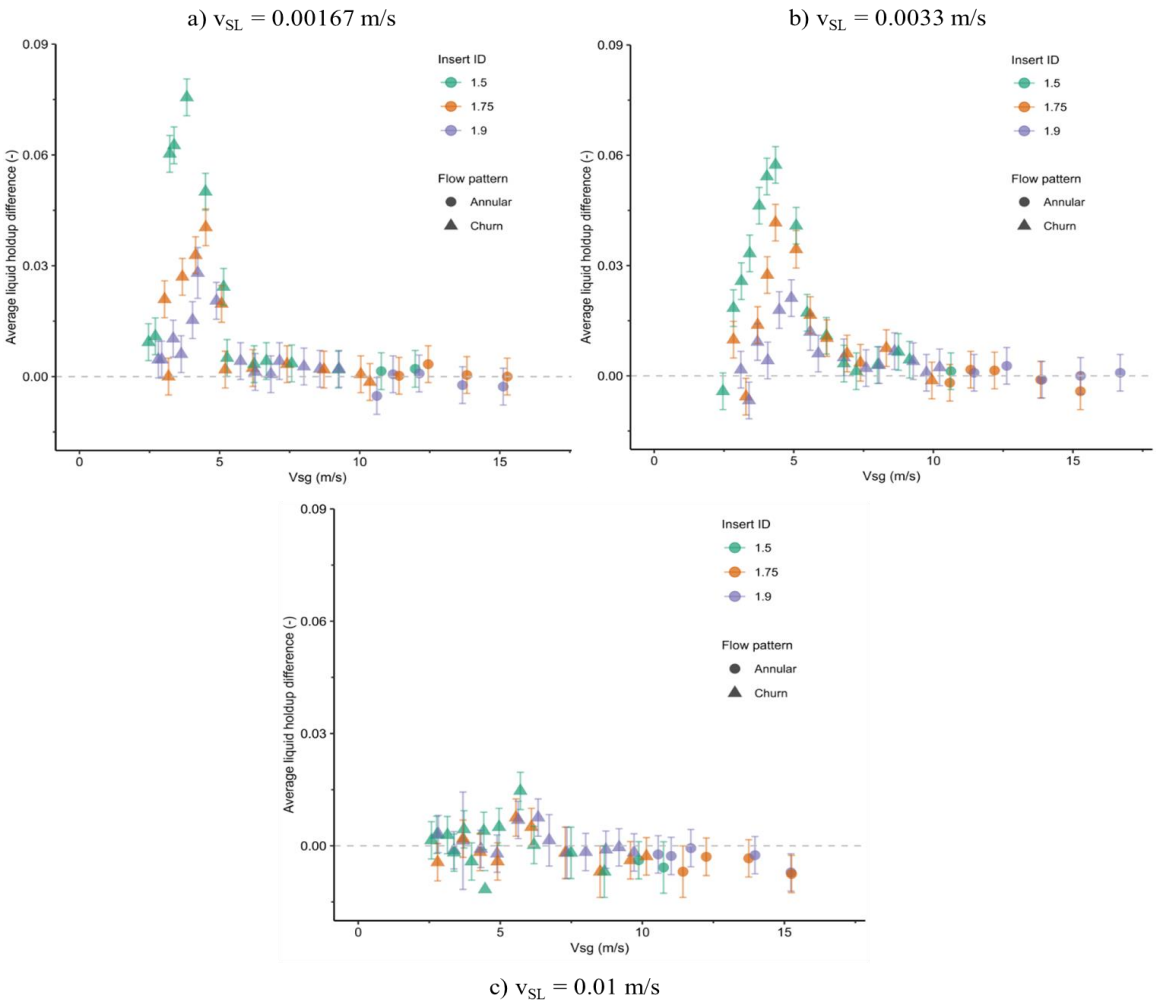

Figure 4.17 Liquid holdup difference vs v_{Sg} with various insert ID's at locations 13

4.2.3. Pressure drop and liquid holdup – Tests with One Insert

With the aim to examine the locality of the insert effects, tests were repeated with a single insert located at the bottom of the test section. Since the tests with 1.9" insert ID did not display significant improvements in comparison to the 1.5" and 1.75" inserts, they were excluded from the experimental design. The results of tests implementing a single insert are discussed below, in a similar way the tests using two inserts were discussed.

Figure 4.18 shows the pressure drop data of the tests with a single insert placed at the bottom section (location 1) with various liquid rates coded by color. Flow patterns are denoted

using circle markers for annular flow and triangle markers for churn flow. Figure 4.18 (a) and (b) correspond to the tests using inserts with 1.5” ID and 1.75” ID, respectively.

Similar to the tests involving two inserts in Figure 4.13, greater v_{SL} results in higher values of pressure drop through all the v_{Sg} values tested. This is explained by a greater proportion of the liquid phase flowing in the test section. The insert ID does not appear to have a significant effect on the pressure drop in these tests, indicated by similarities between Figure 4.18 (a) and Figure 4.18 (b). An explanation for this is the placement of the DP’s above the location where the insert is installed, as shown in Figure 3.2. In contrast, for the tests involving two inserts, at the bottom and top of the test section, the DPs capture the pressure drop across the top insert.

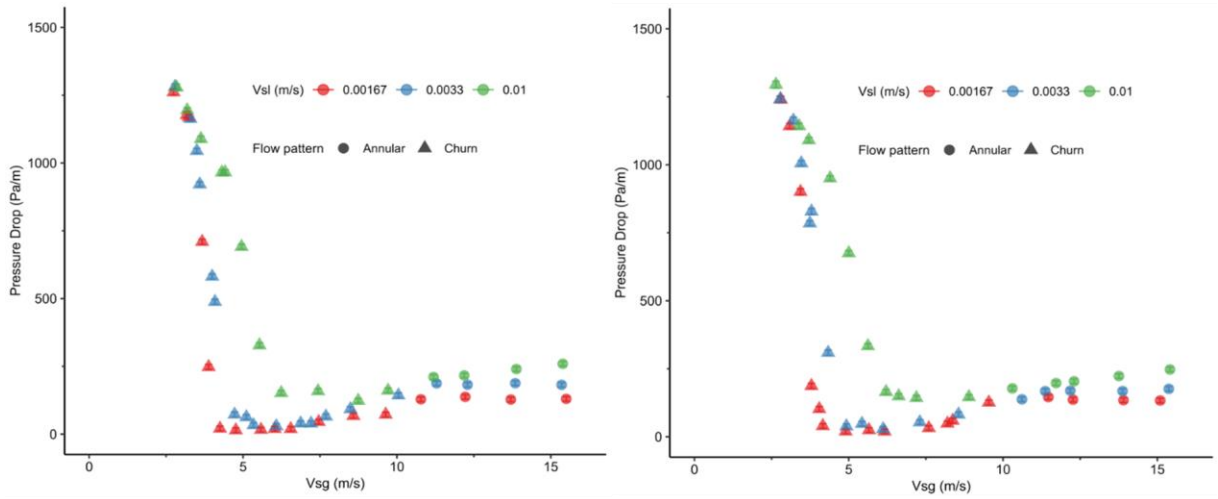

Figure 4.18 Total pressure drop vs v_{Sg} at various liquid rates with one insert

Figure 4.19 exhibits a breakdown of $\left(\frac{dP}{dL}\right)_T$ into its components, $\left(\frac{dP}{dL}\right)_f$ and $\left(\frac{dP}{dL}\right)_G$. Insert ID is indicated using three colors: teal for 1.5”, orange for 1.75”, and purple for 1.9”. It seems that insert ID has no effect on $\left(\frac{dP}{dL}\right)_G$ for any of the liquid rates tested. As expected, when v_{Sg} increases, $\left(\frac{dP}{dL}\right)_G$ term reduces since the liquid holdup decreases approaching annular flow. In contrast with

Figure 4.13, showing the tests with two inserts, positive values are found for $\left(\frac{dP}{dL}\right)_f$ at the low v_{Sg} range. In this region, the insert ID influences $\left(\frac{dP}{dL}\right)_f$ for v_{SL} values of 0.0033 and 0.00167 m/s.

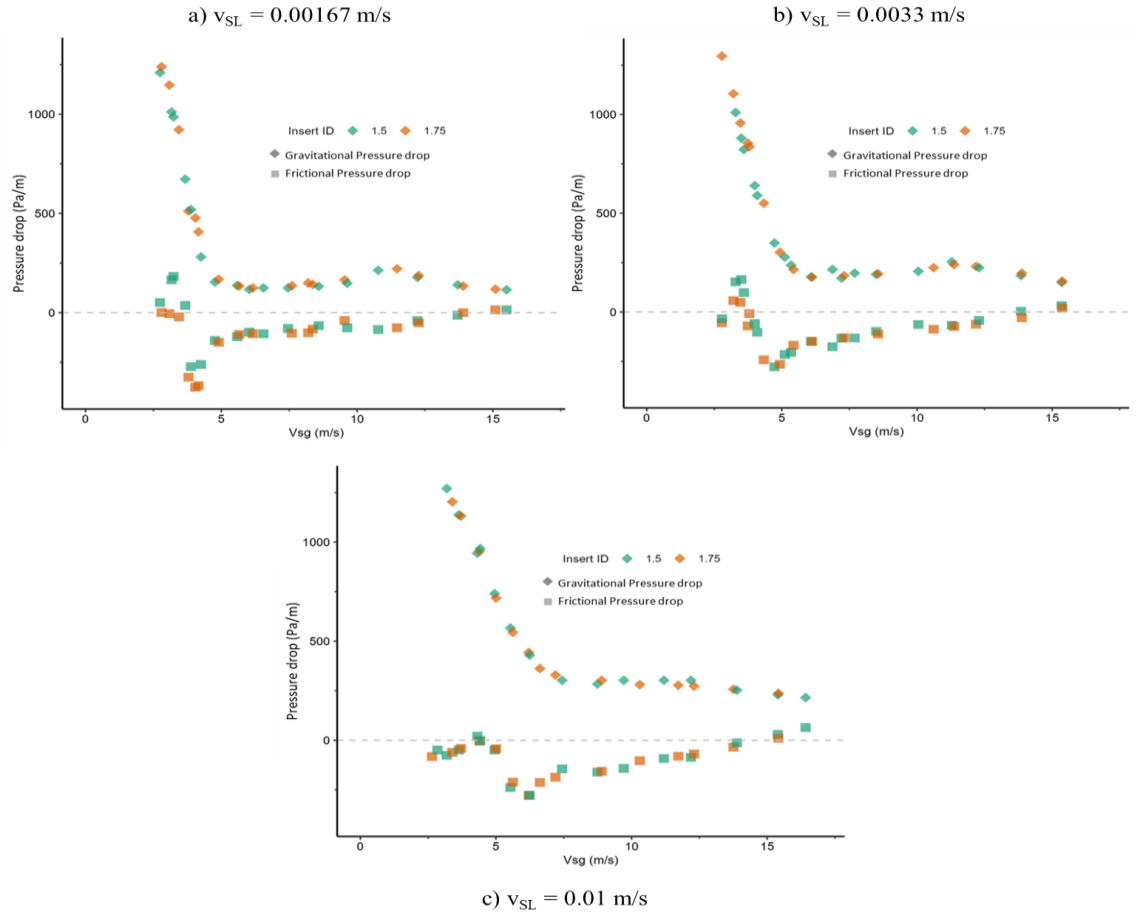

Figure 4.19 Frictional and gravitational pressure drop vs v_{Sg} for various insert ID's at one location

Figure 4.20 depicts the pressure drop difference between tests with various insert sizes and the baseline scenario without inserts. The insert effect on pressure drop is not significant in the annular flow range tested. The negative effect of the inserts, increasing the frictional pressure losses, is not observed here, as the insert is located before the DP sensor at the test section. For v_{SL}=0.01 m/s, Figure 4.20 (c), the use of a single insert negatively affects the pressure drop across

all the gas rates considered. Only for the case of v_{SL} =0.0033 m/s, Figure 4.20 (b), positive results are continuously observed, with an optimum range found in the churn flow region of 3.5<v_{Sg}<6m/s.

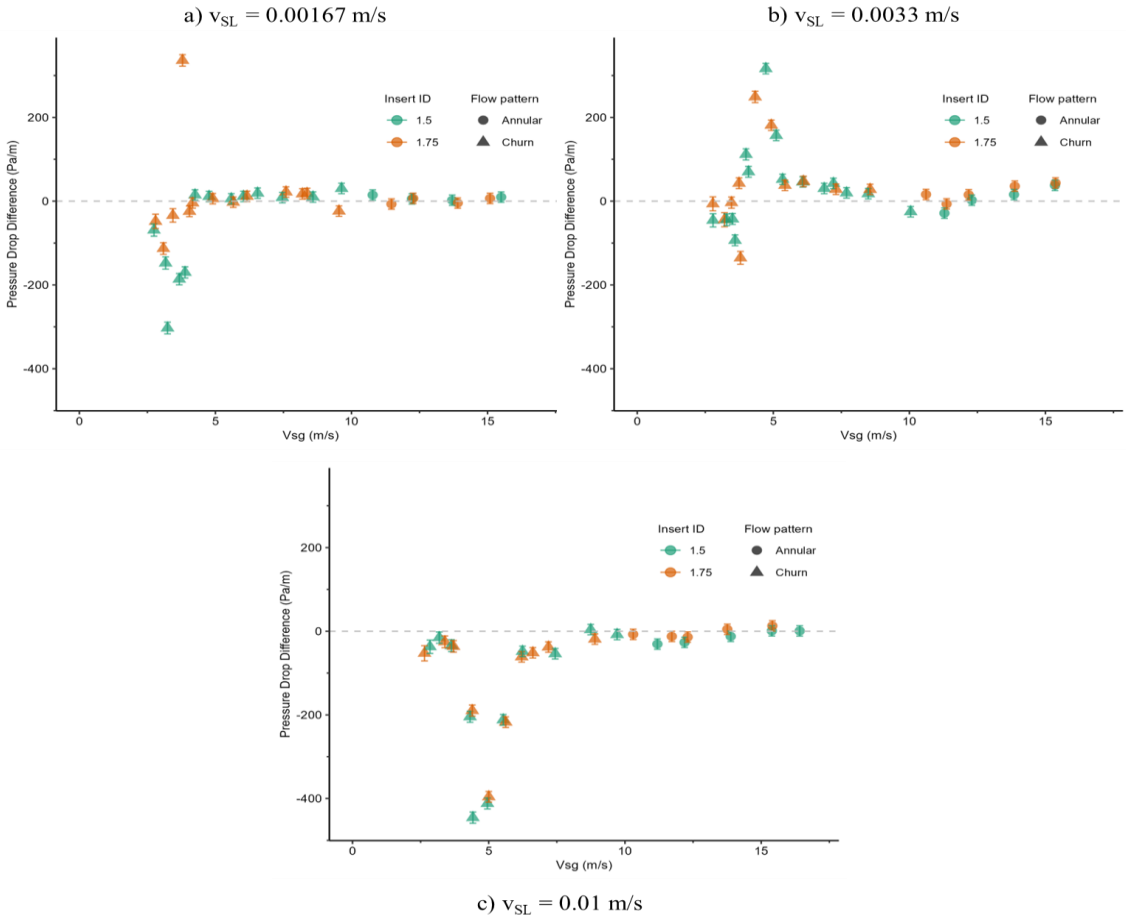

Figure 4.20 Pressure drop difference vs v_{Sg} with various insert ID. Insert location 1

Figure 4.21 illustrates the liquid holdup data of the tests with one insert at various v_{SL} values identified by colors. Flow patterns are indicated with different markers. Figure 4.21 (a) and Figure 4.21 (b) correspond to the tests using inserts with 1.5" and 1.75" ID, respectively. The insert ID does not appear to have a significant effect on the liquid holdup in these tests, as indicated by the similarities between (a) and (b). As expected, higher v_{SL} results in higher liquid holdup (H_L) values for all the cases. The peak with a local maximum H_L previously discussed is also present, and more noticeable at lower v_{SL} values. This peak seems to align with the smallest v_{Sg} value at which the

liquid film does not fall back on the pipe wall. This corresponds to the annular-churn flow transition as observed in the camera recordings.

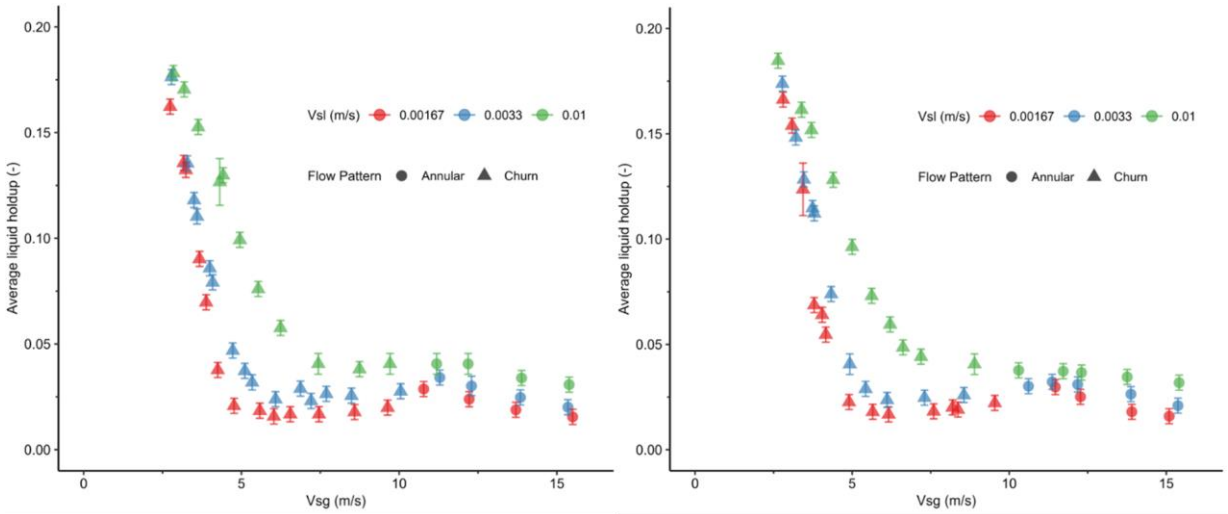

Figure 4.21 Liquid holdup vs v_{Sg} at various liquid rates. Insert location 1

Figure 4.22 shows the liquid holdup difference between tests with various insert sizes and the baseline scenario without inserts. For the low v_{SL} values, the inserts provide improvements in liquid holdup within the churn flow region, a v_{Sg} range of 3-6 m/s. The error bars overlap for inserts of different sizes, indicating that the insert ID is not having a significant effect in this case. However, the results show that even the implementation of a single insert impacts the liquid holdup.

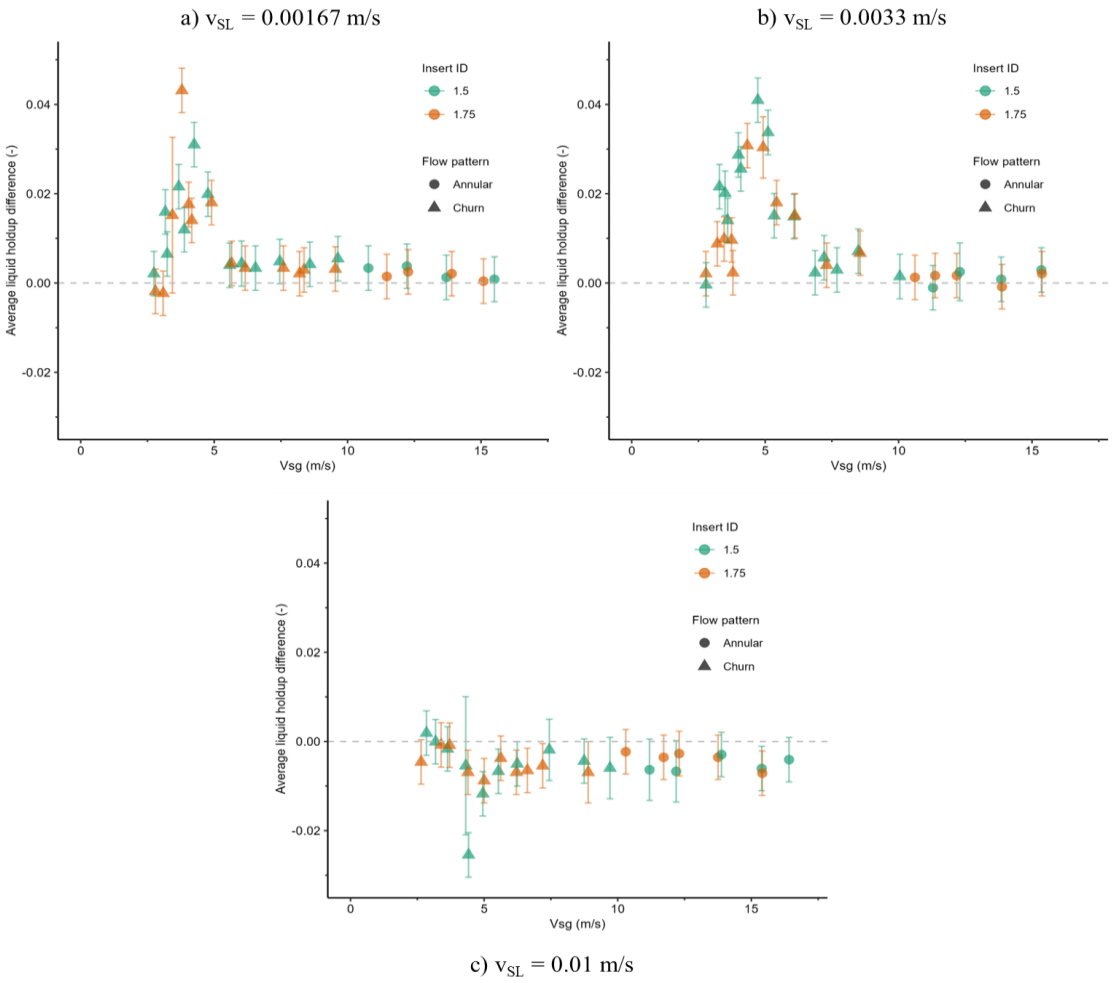

Figure 4.22 Liquid holdup difference vs v_{Sg} with various insert ID's at one location

4.2.4. Pressure drop and liquid holdup – Impact of insert spacing

In this subsection, the analysis shifts its focus to a comparative evaluation of the two insert configurations tested: one insert (location 1) and two inserts (locations 1 and 3). Additionally, the results from a previous study by Alsanea (2022), which explored the use of three inserts (locations 1,2,3), are incorporated in the comparison. This analysis aims to discern the impact of insert spacing, shedding light on the locality of insert effects to optimize liquid lifting. For all the following plots, the liquid rates are coded by color: red for 0.00167 m/s, blue for 0.0033 m/s and green for 0.01 m/s. The insert locations are denoted using different shapes: squares for tests with

one insert placed at location 1, triangles for tests with two inserts placed at locations 1 and 3; filled circles for tests with three inserts, placed at all locations, and empty circles for tests without inserts.

Figure 4.23 shows the pressure drop for tests with different insert spacing setups at several v_{Sg} values and two insert ID's of 1.5" (a) and 1.75" (b). A single v_{SL} is shown in this figure to identify the impact of insert spacing over a wide range of v_{Sg}. For gas rates higher than the minimum pressure drop, or $v_{Sg} > v_{Sg,min}$, the 1.5" ID insert exhibits a greater increasing slope than the 1.75" ID insert. This can be attributed to the increasing pressure losses caused by friction, amplified by the smallest insert opening at higher v_{Sg}.

The main region of interest was identified at the lower v_{Sg} values, where the gravitational losses significantly increase. In this region, around $2.5<v_{Sg}<5$ m/s depending on the liquid rate, the use of inserts shows great improvements in pressure losses, compared to the tests without inserts. Using two inserts instead of three yields a lower pressure drop for both insert sizes at all the tested v_{SL} values. This can be explained by lower frictional pressure losses, as a result of one less insert disturbing the flow, while maintaining the lower levels of gravitational losses.

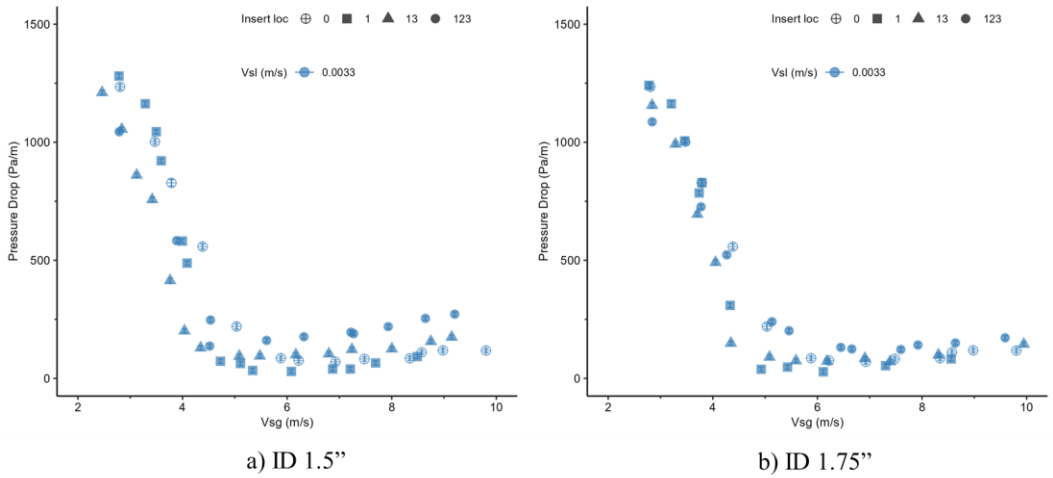

Figure 4.23 Pressure drop vs v_{Sg} for various insert spacing setups and v_{SL}

Figure 4.24 displays the liquid holdup at varying v_{Sg} values tested with different insert spacing setups and two insert ID's of 1.5" (a) and 1.75" (b). As observed before, the liquid holdup is lower at lower v_{SL} values for all the cases, regardless of inserts. In the region of interest, around $2.5<v_{Sg}<5$ m/s, the use of inserts provides significant enhancements over the tests without inserts. This can be appreciated by focusing on a single color, v_{SL}, and noting that the empty circle shapes, no insert tests, yield higher liquid holdup values than the other shapes. The positive effect of the inserts is mainly found at the low v_{SL} values of 0.0033 and 0.00167 m/s.

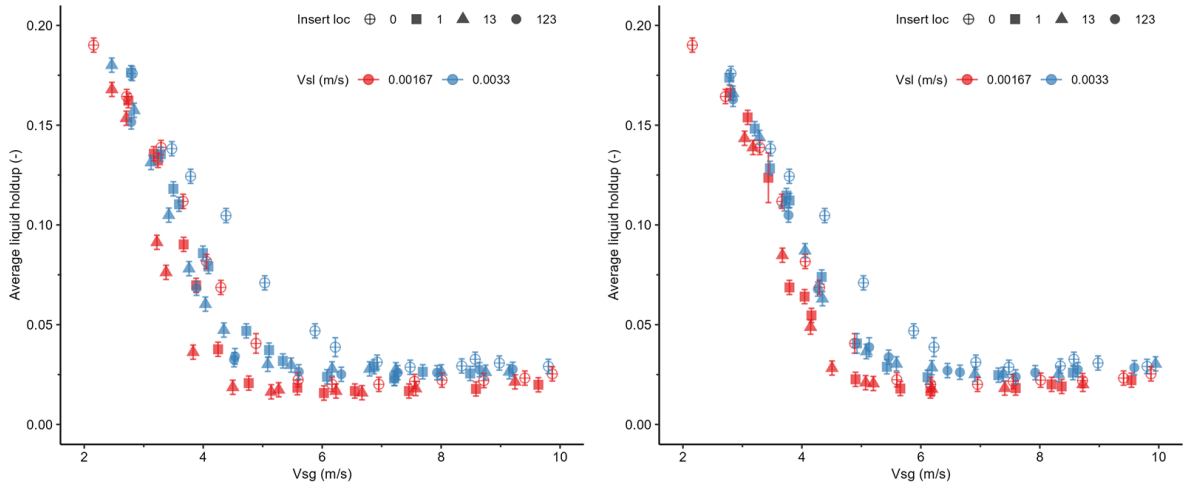

a) ID 1.5" b) ID 1.75"

Figure 4.24 Liquid holdup vs v_{Sg} for various insert spacing setups and v_{SL}

The markers with different shapes, showing different insert spacing cases, overlap for similar v_{SL} values. This suggests that there is no significant difference in the liquid holdup values when using two instead of three inserts. Therefore, using two instead of three inserts would be preferred, since the resulting pressure drop is smaller, while the liquid holdup remains about the same for both inserts tested.

Thus far, it has been established that the use of inserts provides significant improvements in pressure drop and liquid holdup, within a churn flow region. The improvement is characterized

by keeping the pressure drop and liquid holdup values down, after the transition from annular to churn flow, particularly at low v_{SL} values. Also, it was found that two inserts provide better results over the case with three inserts. The presence of three inserts, each representing an added restriction to the flow in a short length, is suboptimal due to the increase of the frictional losses.

Figure 4.25 focuses on the churn flow region, where liquid loading issue begins for the cases with insert locations 1 and 13. The legend used is similar to the one in the previous figures, where v_{SL} is identified by color and the location of the inserts is portrayed with different shapes. Tests are presented with two insert ID's: 1.5" (a) and 1.75" (b). The results indicate that in the region of interest, around $2.5<v_{Sg}<5$ m/s depending on v_{SL}, the use of two inserts provides better outcomes than the use of a single insert. This can be appreciated by focusing on a single color, v_{SL}, and noting that the triangles, test with two inserts, display lower pressure drop values than the squares, corresponding to tests with one insert. It is possible that the use of a single insert is not enough to provide the improvement obtained when using two inserts.

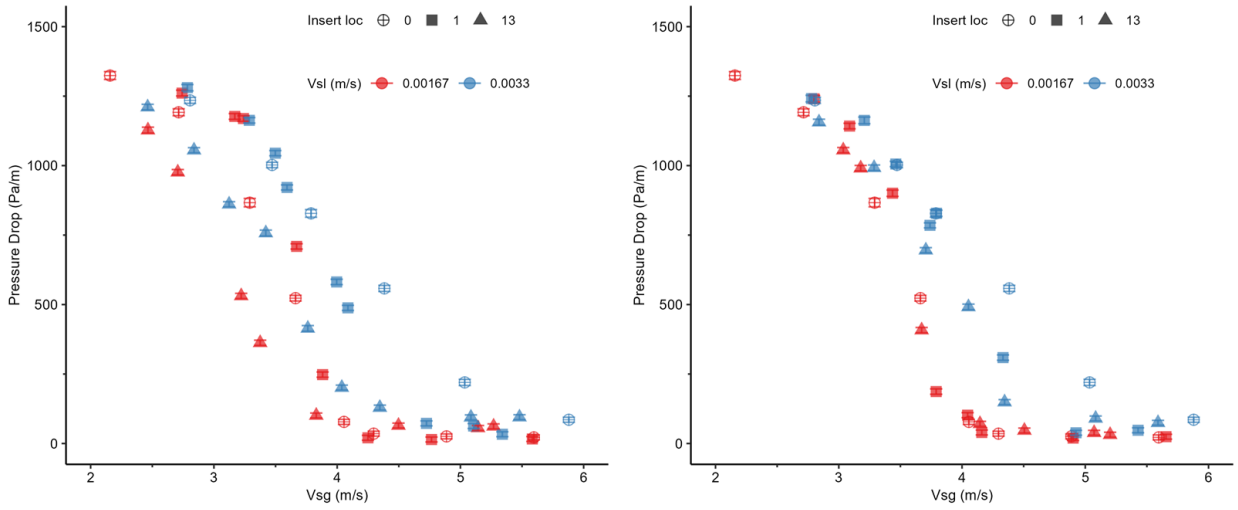

a) ID 1.5" b) ID 1.75"

Figure 4.25 Pressure drop vs v_{Sg} for various insert spacing setups and v_{SL} in churn flow region

Figure 4.26 compares the liquid holdup for the cases with one and two inserts at several v_{Sg} and v_{SL} combinations. Tests with v_{SL}= 0.01 m/s were omitted from this figure as the focus is on insert spacing, and previous analysis indicated that this liquid rate exhibited the smallest improvements. Tests with two insert ID's are presented: 1.5" (a) and 1.75" (b). The results indicate that in the region of interest, around 2.5<v_{Sg}<5 m/s depending on v_{SL}, the use of two inserts provides better outcomes than the use of a single insert. This can be appreciated by focusing on a single color, v_{SL}, and noting that the triangles display lower liquid holdup values than the squares.

In the churn flow region, the gravitational pressure losses dominate. An improvement is observed in liquid holdup with respect to the cases with no inserts. Figure 4.26 results align with those observed in Figure 4.25, as the liquid holdup, related to gravitational pressure losses, is higher in the displayed v_{sg} range when a single insert is used. This results in greater pressure losses when using a single insert compared to using two inserts.

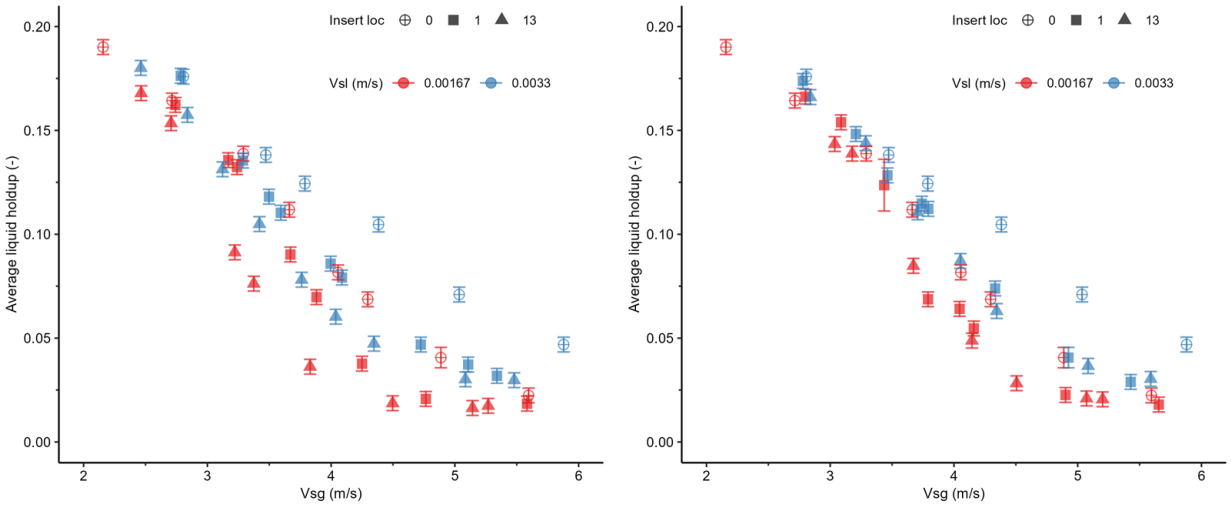

a) ID 1.5"

b) ID 1.75"

Figure 4.26 Liquid holdup vs v_{Sg} for various insert spacing setups and v_{SL} in churn flow region

4.3. Summary of Experimental Results

The impact of inserts on pressure drop becomes adverse at high gas rates, corresponding to annular flow, due to the increased friction. Conversely, at lower gas rates of slug flow, the effect becomes negligible. The inserts exhibit their greatest effectiveness within the churn flow region. Inserts offer notable enhancements in pressure drop and liquid holdup within this critical region. This region is commonly marked by sharp rises in pressure drop and liquid holdup as the v_{Sg} value decreases, immediately following the transition from annular to churn flow. The inserts maintain the liquid holdup and pressure losses at a lower range by increasing the interfacial shear and helping the liquid lifting. This positive effect was observed for a v_{Sg} range of 2.5-5 m/s for the tests of this study, particularly at lower liquid rates.

The tests involving 1.9” ID inserts do not display significant improvements in comparison to the 1.5” and 1.75” inserts. Furthermore, it has been observed that the use of two inserts yields superior outcomes compared to the use of either one or three inserts along the test section. This shows the locality of the insert effects, and the need to place them in regular intervals within the tubing to maintain the liquid lifting performance.

Inserts could promote droplet generation and prevent the fallback of liquid film when strategically placed within the tubing string. The best spacing between inserts for this study was 18 ft, which aligns with the standard lengths of tubular joints, approximately 20ft. This suggests that inserts could be effectively installed at the connections between the joints to maintain the positive effects and address the liquid loading issues.

Fluid properties are expected to influence the effectiveness of inserts in real-life conditions. Lower surface tension, for instance, may facilitate enhanced droplet generation, thereby improving insert efficiency. Further investigation into inserts' performance in deviated wells is required to

fully assess their real-world impacts in gas well operations. Using production data from gas wells in the same reservoir can aid in the design of new wells. For this, one must consider that inserts are effective in the churn flow region, while they cause increased frictional losses in annular flow conditions. This can inform decisions on when to implement inserts for optimal results.

CHAPTER 5. MODELING EVALUATIONS

In this chapter, the evaluation of various models and correlations is undertaken to assess their accuracy in predicting the observed multiphase flow phenomena. This assessment is divided into three main sections. First, a comparison is made between predictions from established commercial models, such as OLGA and TUFFP, and the experimental data for cases without inserts. Second, the performance of existing correlations for predicting liquid loading onset is examined in comparison to the experimental data. Lastly, a mechanistic model developed by Alsanea (2022) is used to calculate the interfacial friction factor for tests with and without inserts. An analysis is conducted on how the presence of inserts affects this factor, required in annular-churn flow models. The analysis quantifies the insert effects on liquid-gas interfacial shear.

5.1. Models Performances

Tulsa University Fluid Flow Project (TUFFP) unified, and OLGA are common commercial models used to predict multiphase flow behavior, pressure, and liquid holdup. Alsanea (2022) developed a model for annular-churn flow which is explained in more detail in Chapter 5.3. The performances of the three models are evaluated using experimental data without inserts. Data from two sources are used for this comparison: the present study, and the study of Alsanea (2022), which was conducted using the same facility. Data points for v_{SL} = 0.00167 m/s correspond to the present study, while most of the data without inserts for v_{SL} values of 0.00033 and 0.01 m/s come from Alsanea's study. This is the same dataset referred to earlier as baseline scenario.

Figure 5.1 displays the comparison between the experimental data and the available models. As reported earlier, higher liquid rates lead to higher pressure drop and liquid holdup values. The flow pattern transition in the commercial models correspond to the inflection point of the curves at v_{Sg} values around 10 m/s. The transition in OLGA (v2019.1) model occurs at higher v_{Sg} when the v_{SL} is increased. On the other hand, TUFFP (v2016) model suggests that the transition occurs closer to v_{Sg}=9m/s for all the v_{SL} values considered.

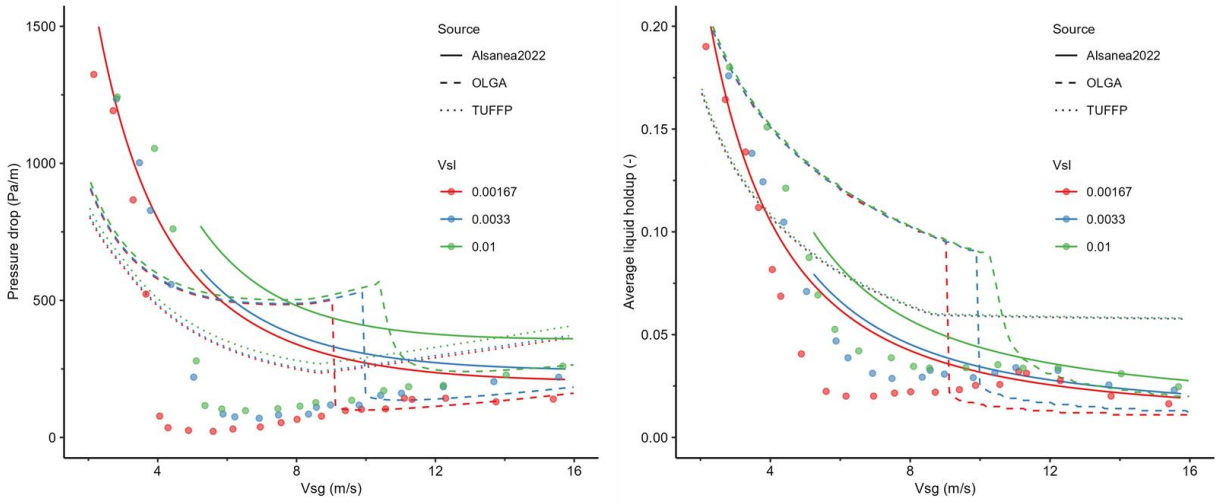

Figure 5.1 Pressure drop, and liquid holdup vs v_{Sg}, experimental data and model predictions

For the lower v_{Sg} values, approaching slug region, both commercial models underpredict the pressure drop. Alsanea's model seems to predict pressure drop with greater accuracy that both commercial models at the lowest v_{Sg} values. At higher v_{Sg} values, in the annular region, TUFFP model overpredicts pressure drop and liquid holdup. OLGA does a better job predicting both parameters, yet slightly underpredicts liquid holdup at low v_{SL} values. Alsanea's model pressure drop prediction falls between the two commercial models in this region, but better captures liquid holdup for the three tested v_{SL}.

The biggest discrepancy is observed in the middle v_{Sg} range of churn flow, where neither of the models can properly convey the experimental results. There is a significant over-prediction by the models for both pressure drop and liquid holdup values in the v_{Sg} range of 5-10 m/s. The discrepancy is amplified at lower v_{SL} values, particularly at 0.00167 m/s. In churn flow region, TUFFP model exhibits the closest alignment to the experimental pressure drop data, while Alsanea's model emerges as the most accurate at predicting liquid holdup.

5.2. Onset of Liquid Loading Prediction

The experimental data were used to assess various models proposed in the literature for predicting the onset of liquid loading (Alsanea et al., 2022; Barnea, 1986; Coleman et al., 1991; Li et al., 2002; Skopich et al., 2015; Turner et al., 1969; Zabaras et al., 1986). These models can be divided into two groups based on their definitions of the liquid loading mechanism. The first group proposes the use of liquid film fallback, while the second category comprises models that suggest droplet fallback as the mechanism. Also, two commercial models were incorporated in the comparison by considering the gas rate at which the predicted flow pattern changes.

The results of models' predictions are shown in Table 5.1. The onset of liquid loading was found at v_{Sg} = 9.38 m/s (30.7 ft/s) by visual observation of the film reversal at v_{SL} = 0.00167 m/s. OLGA and Coleman's models present the lowest errors in the prediction of the liquid loading onset with values of -4% and 8%. Alsanea et al. (2023) reported similar findings for other liquid rates (0.0033, 0.01, 0.02 m/s) and suggested this could be due to the low-pressure conditions of the tests.

Table 5.1 Predictions of the onset of liquid loading for v_{SL}= 0.00167 m/s

Onset of Liquid Loading Models Prediction	**v_{SL} = 0.00167 m/s**	
	v_{Sg} (m/s)	**Relative Error (%)**
Turner et al. (1969)	12.2 (40 ft/s)	30
Minimum pressure drop (Zabaras, 1986)	5.6 18.4	-40
Barnea (1987)	18.7 (61.3 ft/s)	99
Coleman et al. (1991)	10.15 (33.3 ft/s)	8
Li et al. (2002)	4.6 (15.14 ft/s)	-51
Inflection point (Skopich, 2015)	11.3 (37.2 ft/s)	21
OLGA (v2019.1)	9 (29.5 ft/s)	-4
TUFFP (v2016)	20.9 (68.5 ft/s)	123
Positive friction pressure gradient (Alsanea, 2022)	13.7 (45 ft/s)	46

5.3. Interfacial shear stress

Alsanea (2022) proposed a modification to the annular-churn flow mechanistic model by Barnea (1986). This modification incorporated the effect of liquid entrainment in the gas core, which was previously neglected. Figure 5.2 displays a schematic of the proposed model.

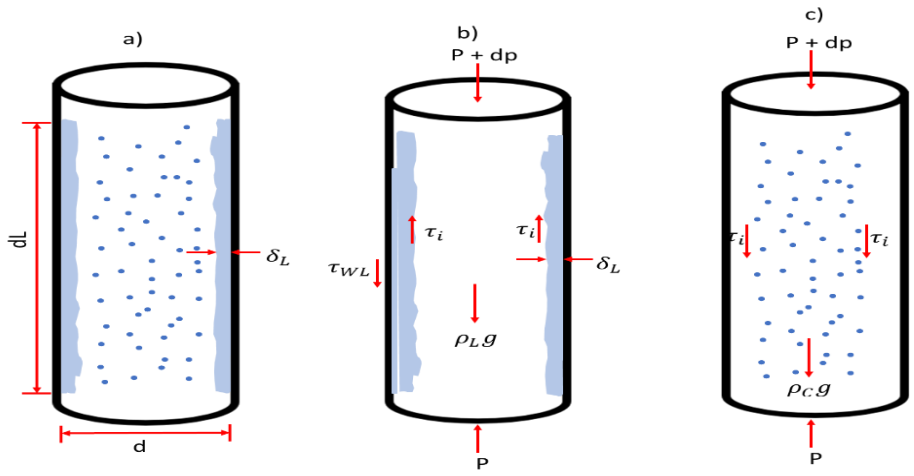

Figure 5.2 Schematic of the proposed model by Alsanea et al. (2022). (a) general schematic, (b) liquid film forces, (c) gas core forces. (Alsanea, 2022)

From Figure 5.2 and considering a uniform film thickness (δ_L), the following geometrical relationships can be obtained.

$$A_F = \pi\delta_L(d - \delta_L) \quad (5.1)$$

$$A_C = \pi(d/2 - \delta_L)^2 \quad (5.2)$$

$$S_L = \pi d \quad (5.3)$$

$$S_I = \pi\,(d - 2\delta_L) \quad (5.4)$$

The momentum balances for gas core and liquid film are defined in Equation (5.5) and Equation (5.6), respectively.

$$-A_C\frac{d_P}{d_L})_C - \tau_i S_I - \rho_C A_C g\ = 0 \quad (5.5)$$

$$-A_F\frac{d_P}{d_L})_F - \tau_{WL} S_L + \tau_i S_I - \rho_L A_F g\ = 0 \quad (5.6)$$

The relevance of the interfacial friction factor, f_i, in the modeling of two-phase flow was discussed in CHAPTER 2. The collected liquid holdup and pressure gradient experimental data

were used to calculate f_i following the next steps. To begin, the area of the liquid (A_L) was determined from the liquid holdup (H_L) definition of Equation (5.7), where A_P refers to the cross-sectional area of the pipe with a constant diameter.

$$H_L = \frac{A_L}{A_P} \tag{5.7}$$

Then, entrainment fraction, f_E, was calculated using the correlation by Oliemans et al. (1986) presented in Equation (2.1). This f_E value depends on fluid properties, flow rates, and pipe diameter. Fluid properties and pipe diameter are constant for the experiments, and the only parameters changing are v_{SL} and v_{Sg}. Core void fraction (α) can then be calculated and used to determine the core density (ρ_C), and viscosity (μ_C) as shown in Equations (5.8) – (5.10). This calculation considers homogeneous no-slip flow between the entrained liquid and the gas core.

$$\alpha_C = \frac{v_{SG}}{v_{SG} + v_{SL} f_E} \tag{5.8}$$

$$\rho_C = \rho_G \alpha_C + \rho_L (1 - \alpha_C) \tag{5.9}$$

$$\mu_C = \mu_G \alpha_C + \mu_L (1 - \alpha_C) \tag{5.10}$$

The f_E value is then used to obtain the area of the liquid film, A_F, as shown in Equation (5.11). In this equation, w_L corresponds to the total mass of the liquid phase, w_{LE} is the mass of entrained liquid, and A_{LE} refers to the area of the entrained liquid.

$$f_E = \frac{w_{LE}}{w_L} = \frac{A_{LE}}{A_L} = \frac{A_L - A_F}{A_L} \tag{5.11}$$

The liquid film thickness, δ_L, is then calculated using the geometrical relationship in Equation (5.1). Using the film thickness, the area of the core and the wetted perimeter are

calculated using Equations (5.2) - (5.4). Then, velocity of the core and velocity of the film are determined using Equation (5.12) and Equation (5.13).

$$v_C = \frac{(v_{SG} + v_{SL} f_E) d^2}{(d - 2\delta_L)^2} \quad (5.12)$$

$$v_F = v_{SL} \frac{(1 - f_E)\, d^2}{4\delta_L (d - \delta_L)} \quad (5.13)$$

With all the components determined, Equation (5.5) can be rearranged to solve for the interfacial shear stress, τ_I. After calculating τ_I, the interfacial friction factor (f_i) is determined with Equation (5.14) as follows.

$$f_i = 2 * \frac{\tau_i}{\rho_c (v_C - v_F)^2} \quad (5.14)$$

Figure 5.3 shows the experimental f_i value calculated using the steps previously described for tests without inserts at v_{SL} = 0.00167 m/s. These values are compared to the predictions of the correlation developed by Alsanea (2022), shown in Equation (2.9). The liquid holdup experimental data are coupled with Alsanea's closure relationship to predict f_i. The results show a relatively good agreement with the experimental data for the low and high ranges of f_i. The greatest relative difference between the predicted and experimental values is found at around f_i = 0.1, corresponding to the v_{Sg} values close to the annular-churn flow transition.

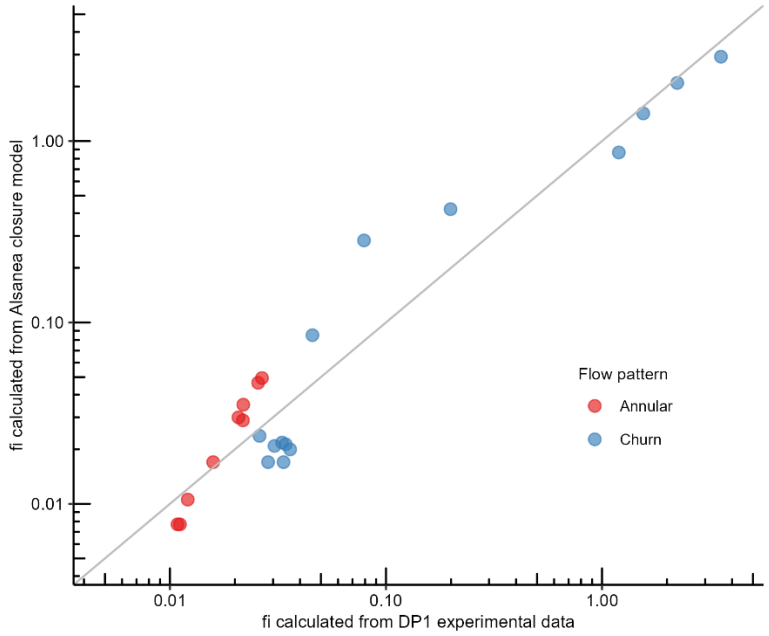

Figure 5.3 Interfacial friction factor for tests without inserts, experimental vs Alsanea closure relationship

The interfacial friction factor was calculated for the tests with inserts to quantify their impacts on multiphase flow behavior. Figure 5.4 depicts the f_i vs v_{Sg} trends for various tests conducted with v_{SL}=0.0033 m/s and one insert (a) or two inserts (b) in the test section.

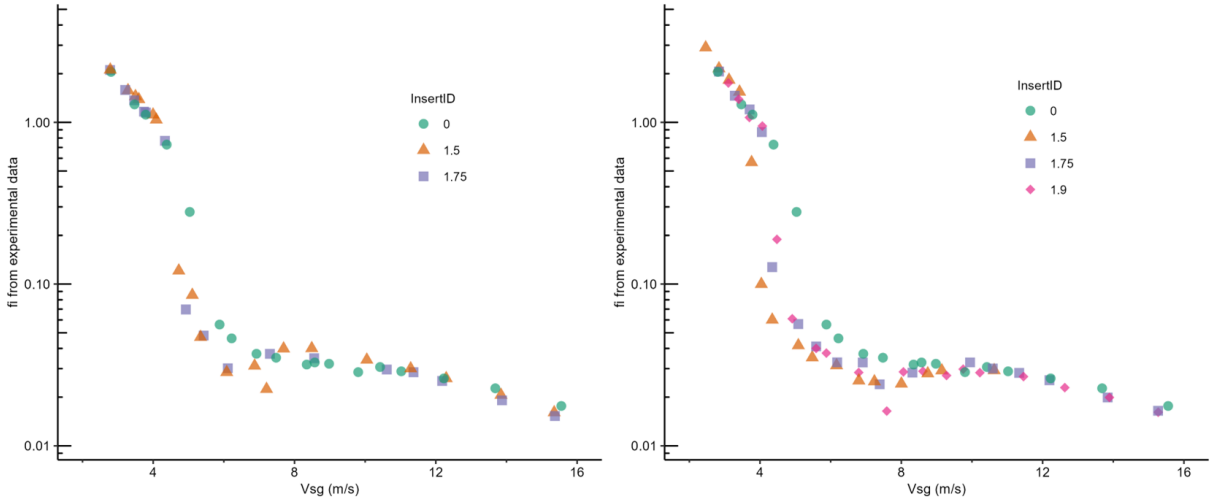

a) Insert at location 1

b) Insert at locations 1,3

Figure 5.4 Interfacial friction factor vs. v_{Sg} for tests at v_{SL} =0.0033 m/s with one insert (a) and two inserts (b)

Similar to the plots for pressure drop and liquid holdup, there is a sharp increase in f_i as the v_{Sg} value drops below 5 m/s. This corresponds to a sharp increase in liquid holdup in this region, approaching slug flow. The tests using inserts show lower f_i values than those without inserts, particularly for the range of $4<v_{Sg}<7$ m/s. In the tests using two inserts, this range extends up to $v_{Sg}=10$ m/s. The f_i calculation involves liquid holdup data, and these values tend to be lower within this range for tests with inserts. The lower holdup results in a thinner liquid film, which is the reason for the reduced f_i. Figure 5.5 shows the back-calculated f_i values from the experimental data, focused on this v_{Sg} range for all the tested v_{SL} values. The triangles show the tests with the 1.5" insert, while the circles show the tests without inserts. The decline in f_i with insert is more apparent for the lower v_{SL} values, which agrees with larger decreases in liquid holdup in such tests after adding the inserts.

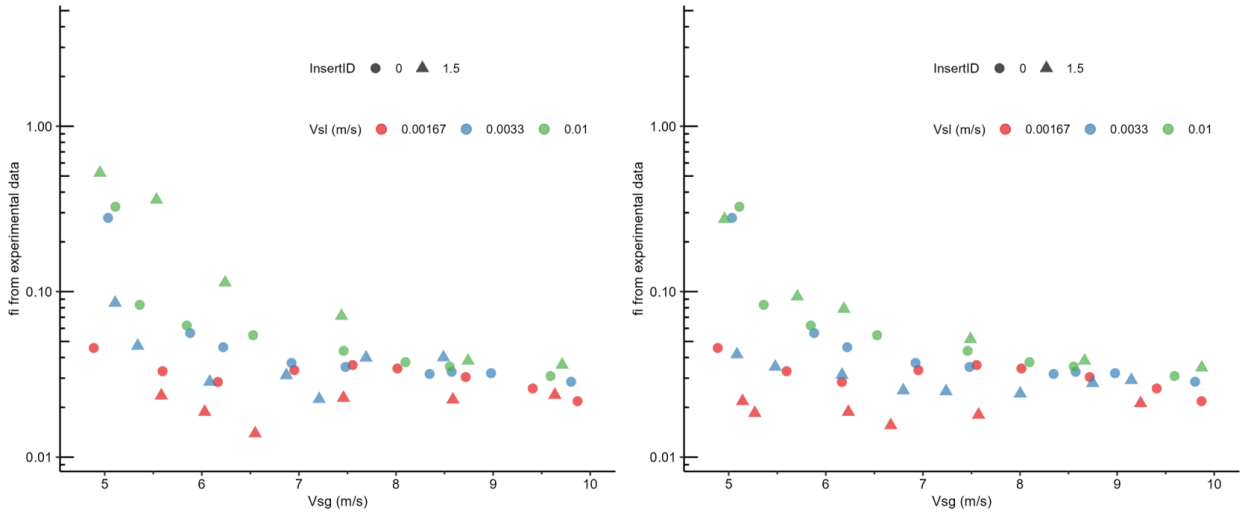

a) Insert at location 1

b) Insert at locations 1,3

Figure 5.5 Interfacial friction factor for tests with inserts area of effect

Figure 5.6 shows the results of using Equation (2.9) proposed by Alsanea to predict f_i using the experimental liquid holdup data in the v_{Sg} range from Figure 5.5. The predictions are compared to the f_i calculated with Equations (5.1) - (5.14) using experimental pressure drop and

liquid holdup measurements. The different liquid rates are differentiated by markers, while the insert sizes used are distinguished by colors. Tests without inserts are shown in blue. A line with slope one is added in both plots to better identify the model's agreement with the experimental data. The dashed lines show prediction errors of ±35%.

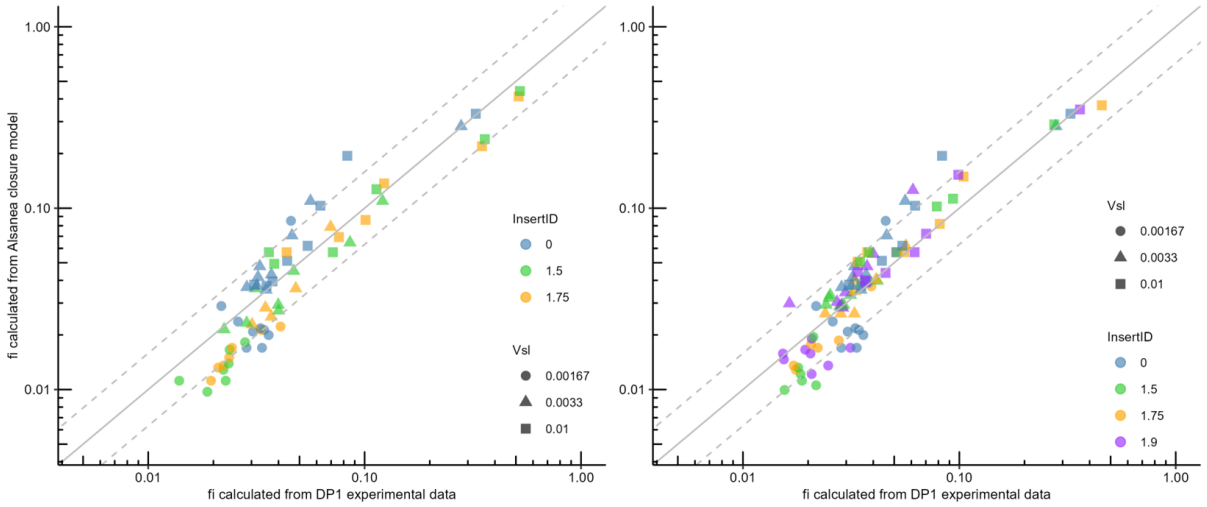

a) Insert at location 1

b) Insert at locations 1,3

Figure 5.6 Interfacial friction factor vs. v_{Sg} log-log for tests at v_{SL}=0.0033 m/s with one insert (a), two inserts (b)

The biggest relative errors are concentrated in the left side of the plot where $f_i < 0.04$. The greatest portion of these tests correspond to those with inserts. From previous plots, these points are in the annular and transition region. Overall, the model's agreement with the fi data seems to be acceptable and within the dashed error lines. However, the model seems to slightly underpredict fi, particularly with inserts. The insert is expected to increase the interfacial shear at the liquid-gas interface, assuming a fixed liquid film thickness. This can be the reason for the underprediction of Alsanea's correlation, which was developed based on tests without inserts.

CHAPTER 6. CONCLUSIONS AND RECOMMENDATIONS

This study is an effort to examine the effects of partial tubing restrictions, namely inserts, on liquid loading in natural gas wells. The conclusions drawn from the conducted experiments are summarized in this chapter. Also, some recommendations are provided for future studies to further explore the effects of this technology on two-phase flow and in the unloading of gas wells.

6.1. Summary and Conclusions

The following conclusions were derived from this research work.

- The effects of partial tubing restrictions, namely inserts, on liquid loading in natural gas wells was studied by considering insert size and spacing. Annular and churn flow regimes were tested, incorporating a wide range of v_{Sg} and 3 v_{SL} values, focusing on low liquid loading conditions.
- Pressure drop curves exhibit a hook shape as v_{Sg} decreases with a sharp increase after a minimum value is encountered at low gas rates in the churn flow region. Both pressure drop and liquid holdup increase when v_{SL} increases.
- Analysis of video recordings revealed the promotion of droplet generation through interactions between the ascending liquid and the inserts. The onset of liquid loading was identified by the reversal of the liquid film on the pipe wall.
- The presence of inserts leads to counteracting effects on pressure drop. On one hand, they lead to a decrease in liquid holdup which results in reduced gravitational losses. On the

other hand, frictional losses increase due to the additional flow restriction caused by the inserts.

- The effectiveness of inserts in altering flow behavior is most pronounced in the churn flow region and at low values of v_{SL}. In these conditions, inserts play a significant role in enhancing droplet generation and preventing liquid film fallback, leading to notable improvements in liquid holdup and pressure drop.
- Comparison of tests with different insert spacing configurations revealed the following performance ranking: Two inserts > One insert > Three inserts. The use of three inserts provided enhancements in liquid holdup but led to significant frictional losses. For one insert tests, there was no substantial improvement in liquid holdup or pressure drop. The use of two inserts offered improved liquid holdup without significant frictional losses.
- The size of inserts is a key factor in their effectiveness, particularly at lower liquid rates and when placed in two locations. Tests involving inserts with a 1.9" inner diameter (ID) did not show significant improvements compared to the 1.75" and 1.5" ID inserts. The 1.5" insert displayed a pronounced positive impact within a narrow operational range, beyond which negative effects on pressure drop were observed. Tests using inserts with a 1.75" ID demonstrated a favorable balance between improvement and operational flexibility.
- At the very low v_{SL} of 0.00167 m/s, Coleman (1991) and OLGA models exhibited better performances in predicting the onset of liquid loading, with errors below 10%. In contrast, the TUFFP and Barnea (1986) models performed poorly, with errors over 100%.
- The comparison of the data with existing models highlights their inadequacy in accurately representing the dynamics of churn flow. These models tend to overpredict both pressure

drop and liquid holdup, particularly at lower v_{SL} values. This underscores the necessity for conducting tests within this range to better understand and characterize churn flow.

- Interfacial shear stress was calculated and the f_i was compared with a model that relies on liquid holdup data for its calculation. The relative error between predicted and experimental values is within an acceptable range, regardless of the presence of inserts. However, the model tends to slightly underpredict the data with the inserts.

6.2. Recommendations

The following recommendations are proposed for future research work.

- Consider examining effects of using different insert sizes in tandem. This approach can optimize liquid holdup improvements while mitigating excessive pressure losses.
- Experiment with different liquids to better understand how properties like surface tension, viscosity, and density impact the effectiveness of inserts implementation in altering flow behavior.
- Explore numerical CFD simulations to gain insights into the two-phase flow behavior with inserts. The presence of inserts influences droplet generation and liquid film stability. A proper simulation method can capture droplet and liquid film dynamics.
- Utilize the extensive dataset collected from the present study to refine mechanistic models and incorporate the effect of inserts. Parameters that must be involved in the model include insert size, spacing between inserts and fluid properties.
- Consider that wells are usually not fully vertical and conduct experiments to investigate how variations in well geometries may influence the behavior of multiphase flow systems where inserts are present.

- Investigate the use of artificial neural networks (ANNs) for flow pattern recognition using the collected video database with over 500 vertical two-phase flow tests. Ensure future tests maintain standardized camera positions and consistent lighting conditions to enhance video comparability for more accurate ANN training and validation.
- Conduct pilot-scale experiments in natural gas wells to bridge the gap between laboratory results and real-world scenarios. This kind of validation may help to identify other important variables.

NOMENCLATURE

Symbol	Meaning	Units
A_C	Area of gas core	m^2
A_F	Area of liquid film	m^2
A_L	Cross sectional area of liquid	m^2
A_P	Cross sectional area of pipe	m^2
d	Internal pipe diameter	m
d^*	Dimensionless coefficient proposed by Bharatan and Wallis (1983)	-
$\left(\frac{dP}{dL}\right)_f$	Frictional pressure drop gradient	Pa/m
$\left(\frac{dP}{dL}\right)_G$	Gravitational pressure drop gradient	Pa/m
$\left(\frac{dP}{dL}\right)_T$	Total pressure drop gradient	Pa/m
f_E	Entrainment fraction	-
f_i	Interfacial friction factor	-
g	Gravity force	m/s^2
h_L	Height of liquid column	m
h_{Total}	Total height of test section	m
H_L	Liquid holdup	-
ID	Internal diameter of insert	in
$\dot{m}$	Mass flow rate of air	kg/s
P	Pressure	Pa
QCV	Quick Closing Valve	/
R	Universal gas constant (8.314)	J/(mol.K)
R_{air}	Specific gas constant for air	J/(kg.K)
S_I	Wetted perimeter of core phase	m
S_L	Pipe perimeter	m
T	Temperature	K
t	Time	s
v_F	Liquid film velocity	m/s
v_C	Core velocity	m/s

v_{Sg}	Superficial gas velocity	m/s
$v_{Sg,min}$	Superficial gas velocity at minimum pressure drop	m/s
v_{SL}	Superficial liquid velocity	m/s
w_L	Total mass of liquid flowing	kg
w_{LE}	Mass of liquid entrained	kg
α_C	Core void fraction	-
δ_L	Liquid film thickness	m
ρ_A	Air density	kg/m^3
ρ_C	Core density	kg/m^3
ρ_L	Liquid density	kg/m^3
ρ_L	Liquid density	kg/m^3
μ_C	Core viscosity	Pa.s
σ	Surface tension	N/m
τ_I	Interfacial shear stress	Pa
τ_{WL}	Wall shear stress	Pa

REFERENCES

Alsanea, M. (2018). *Effect of water cut on onset of liquid loading and foam lift performance in horizontal well*. The University of Tulsa.

Alsanea, M. (2022). *Effects of restrictions and liquid properties on liquid loading in natural gas wells* [University of Oklahoma]. https://shareok.org/handle/11244/336894

Alsanea, M., Mateus-Rubiano, C., & Karami, H. (2022). Liquid Loading in Natural Gas Vertical Wells: A Review and Experimental Study. *SPE Production & Operations*, *37*(03), 554–571. https://doi.org/10.2118/209819-PA

Alsanea, M., Mateus-Rubiano, C., & Karami, H. (2023). Experimental study on the effect of liquid properties on fluid behavior and liquid loading in vertical natural gas wells. *Geoenergy Science and Engineering*, *230*, 212180. https://doi.org/10.1016/j.geoen.2023.212180

Ansari, A. M., Sylvester, N. D., Sarica, C., Shoham, O., & Brill, J. P. (1994). A Comprehensive Mechanistic Model for Upward Two-Phase Flow in Wellbores. *SPE Production & Facilities*, *9*(02), 143–151. https://doi.org/10.2118/20630-PA

Aziz, K., & Govier, G. W. (1972). Pressure Drop In Wells Producing Oil And Gas. *Journal of Canadian Petroleum Technology*, *11*(03). https://doi.org/10.2118/72-03-04

Azzopardi, B. J., & Wren, E. (2004). What is entrainment in vertical two-phase churn flow? *International Journal of Multiphase Flow*, *30*(1), 89–103. https://doi.org/10.1016/j.ijmultiphaseflow.2003.11.001

Barnea, D. (1986). Transition from annular flow and from dispersed bubble flow—unified models for the whole range of pipe inclinations. *International Journal of Multiphase Flow*, *12*(5), 733–744. https://doi.org/10.1016/0301-9322(86)90048-0

Barnea, D., Shoham, O., & Taitel, Y. (1980). Flow pattern characterization in two phase flow by electrical conductance probe. *International Journal of Multiphase Flow*, *6*(5), 387–397. https://doi.org/10.1016/0301-9322(80)90001-4

Barreto, C. V., Karami, H., Pereyra, E., & Sarica, C. (2017, July 30). *Effect of Surfactant (Foamer) Delivery Location on Horizontal Wells Deliquification*. https://doi.org/10.1115/FEDSM2017-69512

Beggs, D. H., & Brill, J. P. (1973). A Study of Two-Phase Flow in Inclined Pipes. *Journal of Petroleum Technology*, *25*(05), 607–617. https://doi.org/10.2118/4007-PA

Belfroid, S. P. C., Schiferli, W., Alberts, G. J. N., Veeken, C. A. M., & Biezen, E. (2008). Prediction Onset and Dynamic Behaviour of Liquid Loading Gas Wells. *All Days*, 21–24. https://doi.org/10.2118/115567-MS

Bharathan, D., & Wallis, G. B. (1983). Air-water countercurrent annular flow. *International Journal of Multiphase Flow*, *9*(4), 349–366. https://doi.org/10.1016/0301-9322(83)90093-9

Caetano, E. F. (1985). *Upward vertical two-phase flow through an annulus* [The University of Tulsa]. https://www.osti.gov/biblio/5277340

Chaves, G. S., Karami, H., Ferreira Filho, V. J. M., & Vieira, B. F. (2022). A comparative study on the performance of multiphase flow models against offshore field production

data. *Journal of Petroleum Science and Engineering*, *208*, 109762. https://doi.org/10.1016/j.petrol.2021.109762

Coleman, S. B., Clay, H. B., McCurdy, D. G., & Norris, L. H. (1991). A New Look at Predicting Gas-Well Load-Up. *Journal of Petroleum Technology*, *43*(03), 329–333. https://doi.org/10.2118/20280-PA

Devshali, S., Manchalwar, V., Deuri, B., Malhotra, S. K., Prasad, B. V. R. V., Yadav, M., Kumar, A., & Uniyal, R. (2019). Revisiting old sands with a different perspective – A pragmatic approach for maximizing recovery from gas reservoirs. *Society of Petroleum Engineers - SPE Oil and Gas India Conference and Exhibition 2019, OGIC 2019*. https://doi.org/10.2118/194600-ms

Duns, H. , J., & Ros, N. C. J. (1963). Vertical flow of gas and liquid mixtures in wells. *6th World Petroleum Congress*. http://onepetro.org/WPCONGRESS/proceedings-pdf/WPC06/All-WPC06/WPC-10132/2079811/wpc-10132.pdf/1

Energy Institute. (2023). *Statistical Review of World Energy*. https://www.energyinst.org/statistical-review

Faghri, A., & Zhang, Y. (2020). *Fundamentals of Multiphase Heat Transfer and Flow*. Springer International Publishing. https://doi.org/10.1007/978-3-030-22137-9

Falcone, G., Teodoriu, C., Reinicke, K. M., & Bello, O. O. (2008). Multiphase-Flow Modeling Based on Experimental Testing: An Overview of Research Facilities Worldwide and the Need for Future Developments. *SPE Projects, Facilities & Construction*, *3*(03), 1–10. https://doi.org/10.2118/110116-PA

Hagedorn, A. R., & Brown, K. E. (1965). Experimental Study of Pressure Gradients Occurring During Continuous Two-Phase Flow in Small-Diameter Vertical Conduits. *Journal of Petroleum Technology*, *17*(04), 475–484. https://doi.org/10.2118/940-PA

Hanafizadeh, P., Shahani, A., Ghanavati, A., & Akhavan-Behabadi, M. A. (2017). Experimental investigation of air-water-oil three-phase flow patterns in inclined pipes. *Experimental Thermal and Fluid Science*, *84*, 286–298. https://doi.org/10.1016/j.expthermflusci.2017.02.009

Hewitt, G. F., & Hall-Taylor, N. S. (1970). *Annular Two-phase Flow* ([1st ed.].). Elsevier. https://doi.org/10.1016/C2009-0-06773-7

Jayanti, S., & Brauner, N. (1994). Churn flow. *Multiphase Science and Technology*, *8*(1–4), 471–521. https://doi.org/10.1615/MultScienTechn.v8.i1-4.90

Karami, H., Torres, C. F., Pereyra, E., & Sarica, C. (2016). Experimental Investigation of Three-Phase Low-Liquid-Loading Flow. *Oil and Gas Facilities*, *5*(02), 45–56. https://doi.org/10.2118/174926-PA

Lea, J. F., & Rowlan, L. (2019). *Gas Well Deliquification*. Elsevier. https://doi.org/10.1016/C2017-0-04099-5

Li, M., Li, S. L., & Sun, L. T. (2002). New View on Continuous-Removal Liquids From Gas Wells. *SPE Production & Facilities*, *17*(01), 42–46. https://doi.org/10.2118/75455-PA

Mateus-Rubiano, C. A., Alsanea, M., & Karami, H. (2023, April 17). An Experimental Study on the Effects of Tubular Restrictions on Liquid Lifting in Natural Gas Wells. *SPE Oklahoma City Oil and Gas Symposium*. https://doi.org/10.2118/213063-MS

Nosseir, M. A., Darwich, T. A., Sayyouh, M. H., & El Sallaly, M. (1997, March 9). A New Approach for Accurate Prediction of Loading in Gas Wells Under Different Flowing Conditions. *All Days*. https://doi.org/10.2118/37408-MS

Oliemans, R. V. A., Pots, B. F. M., & Trompé, N. (1986). Modelling of annular dispersed two-phase flow in vertical pipes. *International Journal of Multiphase Flow*, *12*(5), 711–732. https://doi.org/10.1016/0301-9322(86)90047-9

Park, H. Y., Falcone, G., & Teodoriu, C. (2009). Decision matrix for liquid loading in gas wells for cost/benefit analyses of lifting options. *Journal of Natural Gas Science and Engineering*, *1*(3), 72–83. https://doi.org/10.1016/j.jngse.2009.03.009

Putra, S. (2000). *Development of a mechanistic two-fluid churn flow model and design of tubing-collar inserts for enhancing liquid lifting to prevent liquid load-up in gas wells*. Colorado School of Mines.

Putra, S., & Christiansen, R. (2001). Design of Tubing Collar Inserts for Producing Gas Wells Below Their Critical Velocity. *Proceedings of SPE Annual Technical Conference and Exhibition*, 1941–1956. https://doi.org/10.2523/71554-MS

Shoham, O. (2006). *Mechanistic Modeling of Gas-Liquid Two-Phase Flow in Pipes*. Society of Petroleum Engineers. https://doi.org/10.2118/9781555631079

Skopich, A. ., Pereyra, E. ., Sarica, C. ., & Kelkar, M. . (2015). Pipe-Diameter Effect on Liquid Loading in Vertical Gas Wells. *SPE Production & Operations*, *30*(02), 164–176. https://doi.org/10.2118/164477-PA

Sylvester, N. D. (1987). A Mechanistic Model for Two-Phase Vertical Slug Flow in Pipes. *Journal of Energy Resources Technology*, *109*(4), 206–213. https://doi.org/10.1115/1.3231348

Taitel, Y., Barnea, D., & Dukler, A. E. (1980). Modelling flow pattern transitions for steady upward gas-liquid flow in vertical tubes. *AIChE Journal*, *26*(3), 345–354. https://doi.org/10.1002/aic.690260304

Takano, S., Masanobu, S., Kanada, S., & Ono, M. (2023). Correlation for calculating frictional pressure drops in vertical three-phase flows for subsea-resource production. *Ocean Engineering*, *275*, 114121. https://doi.org/10.1016/j.oceaneng.2023.114121

Tugan, M. F. (2020). Deliquification techniques for conventional and unconventional gas wells: Review, field cases and lessons learned for mitigation of liquid loading. *Journal of Natural Gas Science and Engineering*, *83*(July), 103568. https://doi.org/10.1016/j.jngse.2020.103568

Turner, R. G., Hubbard, M. G., & Dukler, A. E. (1969). Analysis and Prediction of Minimum Flow Rate for the Continuous Removal of Liquids from Gas Wells. *Journal of Petroleum Technology*, *21*(11), 1475–1482. https://doi.org/10.2118/2198-PA

US Energy Information Administration. (2023). *Monthly Energy Review - September*. www.eia.gov/mer

Veeken, C. A. M. . A. M., & Belfroid, S. P. C. . P. C. (2011). New Perspective on Gas-Well Liquid Loading and Unloading. *SPE Production & Operations*, *26*(04), 343–356. https://doi.org/10.2118/134483-PA

Wallis, G. B. (1969). *One-dimensional Two-phase Flow*. McGraw-Hill.

Yamamoto, H., & Christiansen, R. (1999, May). Enhancing Liquid Lift From Low Pressure Gas Reservoirs. *Proceedings of SPE Rocky Mountain Regional Meeting*. https://doi.org/10.2523/55625-MS

Yaqub, M. W., Marappagounder, R., Rusli, R., D.M., R. P., & Pendyala, R. (2020). Review on gas–liquid–liquid three–phase flow patterns, pressure drop, and liquid holdup in pipelines. *Chemical Engineering Research and Design*, *159*, 505–528. https://doi.org/10.1016/j.cherd.2020.04.029

Zabaras, G., Dukler, A. E., & Moalem-Maron, D. (1986). Vertical upward cocurrent gas-liquid annular flow. *AIChE Journal*, *32*(5), 829–843. https://doi.org/10.1002/aic.690320513

Zhang, H.-Q., Wang, Q., Sarica, C., & Brill, J. P. (2003). Unified Model for Gas-Liquid Pipe Flow via Slug Dynamics—Part 1: Model Development. *Journal of Energy Resources Technology*, *125*(4), 266–273. https://doi.org/10.1115/1.1615246

APPENDIX A

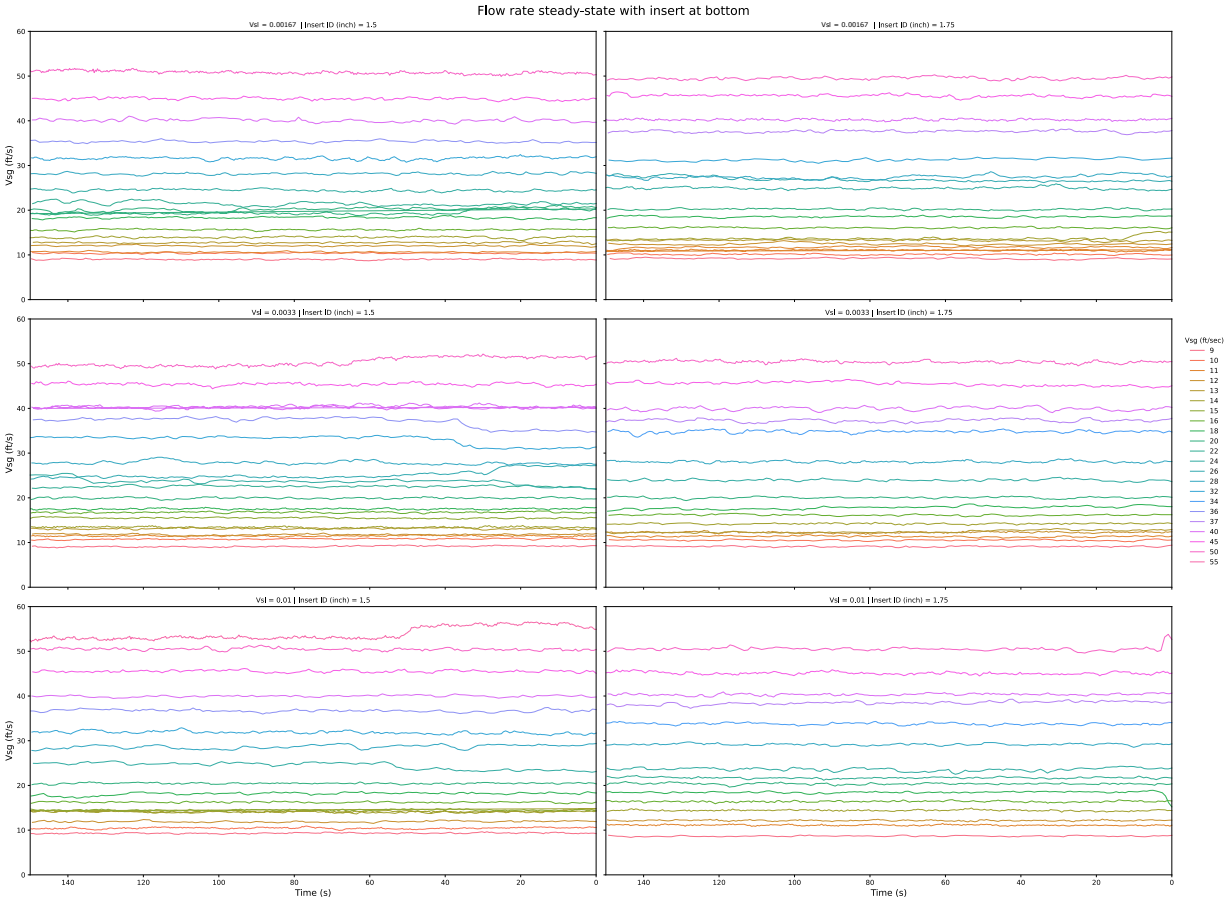

Figure A.1 Air flowrate fluctuations for tests with insert at bottom location

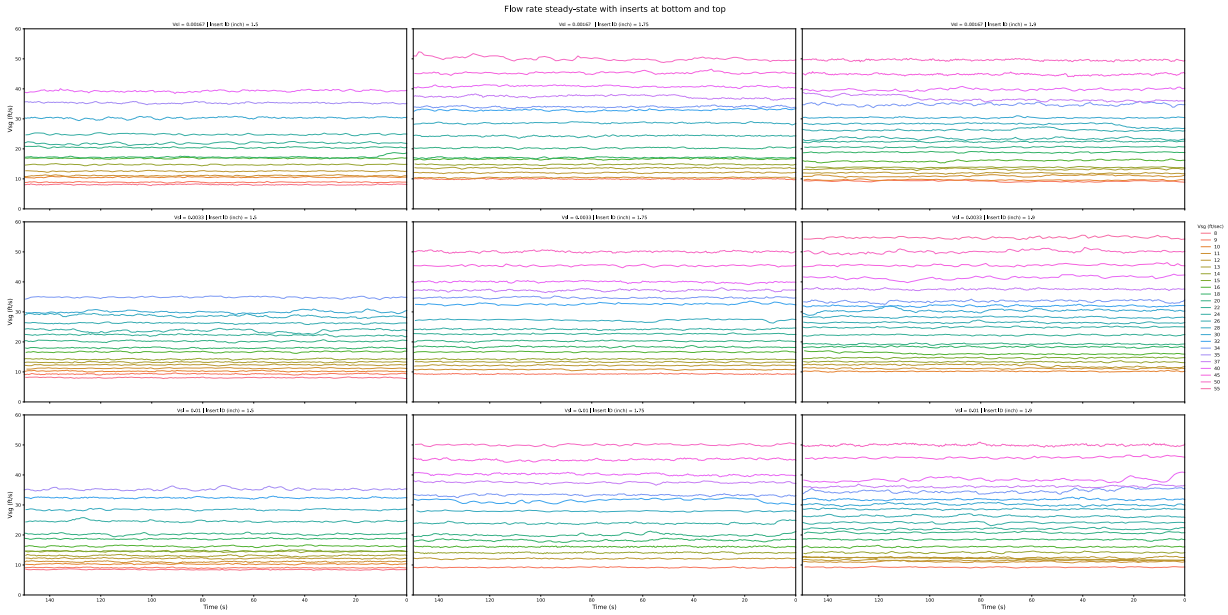

Figure A.2 Air flowrate fluctuations for tests with inserts at bottom and top locations simultaneously